NASA TN D-347

TECHNICAL NOTE

D-347

ON THE INDUCED FLOW OF AN ELECTRICALLY CONDUCTING LIQUID IN A RECTANGULAR DUCT BY ELECTRIC AND MAGNETIC FIELDS OF FINITE EXTENT

By Vernon J. Rossow, Wm. Prichard Jones,
and Robert H. Huerta

Ames Research Center
Moffett Field, Calif.

NATIONAL AERONAUTICS AND SPACE ADMINISTRATION
WASHINGTON
January 1961

NATIONAL AERONAUTICS AND SPACE ADMINISTRATION

TECHNICAL NOTE D-347

ON THE INDUCED FLOW OF AN ELECTRICALLY CONDUCTING LIQUID IN A RECTANGULAR DUCT BY ELECTRIC AND MAGNETIC FIELDS OF FINITE EXTENT

By Vernon J. Rossow, Wm. Prichard Jones,
and Robert H. Huerta

SUMMARY

Reported here are the results of a systematic study of a model of the direct-current electromagnetic pump. Of particular interest is the motion imparted to the electrically conducting fluid in the rectangular duct by the body forces that result from applied electric and magnetic fields. The purpose of the investigation is to associate the observed fluid motion with the characteristics of the electric and magnetic fields which cause them. The experiments were carried out with electromagnetic fields that moved a stream of copper sulphate solution through a clear plastic channel. Ink filaments injected into the stream ahead of the region where the fields were applied identify the motion of the fluid elements as they passed through the test channel. Several magnetic field configurations were employed with a two-dimensional electric current distribution in order to study and identify the magnitude of some of the effects on the fluid motion brought about by nonuniformities in the electromagnetic fields. A theoretical analysis was used to guide and evaluate the identification of the several fluid motions observed. The agreement of the experimental data with the theoretical predictions is satisfactory. It is found that sizable variations in the velocity profile and pressure head of the output stream are produced by the shape of the electric and magnetic fields.

INTRODUCTION

A given electric current and magnetic field will exert the same force on a fluid in a container as on a wire in an electric motor. A difference exists, however, in that the wires are constrained to move in one predetermined direction, whereas, the fluid is free to move in any direction permitted by its boundaries. As a result, particular characteristics of the imposed fields are displayed in the fluid motion, and complex flow patterns may arise. If the individual motions imparted to the fluid can can be associated with particular features of the applied fields, modifications can be made to the structure of the magnet, electrodes, or channel to tailor the flow to fit a particular need. The purpose of this

investigation was to construct and operate experimental apparatus in which it would be possible to observe the fluid motions and to identify these with the impressed fields by means of theoretical considerations. In this way, the information on the characteristics of electromagnetic flow devices is extended by the quantitative theoretical and experimental treatment of the fluid motion reported here.

In order to realize a simple configuration for the present study that would be amenable to analysis and for which experimental results could be obtained, the arrangement shown in sketch (a) was chosen. It is basically a laboratory model of direct-current electromagnetic pumps (see appendix A) which are in use in various industries. The electric and magnetic fields are produced by an iron-core electromagnet and by two copper electrodes embedded in the channel sides. A two-dimensional current distribution is achieved by extending the electrodes the full depth, d, of a rectangular duct made of transparent plastic. The copper sulphate solution, used as the working fluid, flows at a velocity from 1 to 4 inches per second under the influence of 0.4 to 1.6 amperes current and a magnetic field of about 4000 gauss. Since both the fluid and channel are transparent, motion of the liquid is visualized by injecting seven ink filaments periodically into the centerplane of the stream.

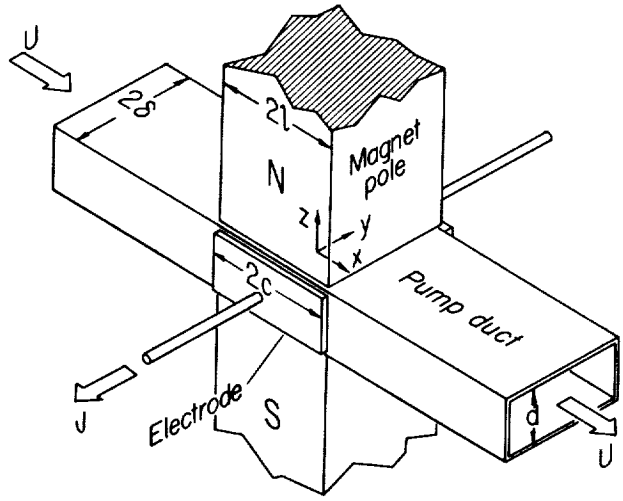

Sketch (a)

The electric current and flow rate for the tests are sufficiently low that the secondary or induced magnetic and electric fields are more than 10^{-3} times smaller than the primary or externally imposed fields. Numerical values for several of the dimensionless parameters that characterize the flow field are

$$\text{Hartmann parameter} = \sqrt{\frac{\sigma}{\eta}}\, B\delta \approx 10^{-2}$$

$$\text{Applied/counter (or back) emf} = \frac{E}{UB} \approx 10^{3}$$

$$\text{Magnetic Reynolds number} = \sigma\mu U\delta \approx 10^{-8}$$

$$\text{Viscous Reynolds number} = \frac{\delta U}{\nu} = 300 \text{ to } 1000$$

where U, η, ν, μ, and σ are the fluid velocity, viscosity, kinematic viscosity, magnetic permeability, and electrical conductivity, respectively. The quantities B and δ are the magnetic field strength and the characteristic length of the flow field.

Presented here are the results of a systematic series of tests and of a theoretical study carried out on the device shown schematically in sketch (a) and in figure 1. Various flow phenomena that appeared in the tests are associated with certain features of the impressed fields. Local values for the pressure head of the fluid as obtained from theoretical expressions are compared with the measured results to corroborate these associations. A resumé of the literature is presented in appendix A.

A
2
7
6

A description of some of the results of this investigation was presented at the International Symposium on Magneto-Fluid Dynamics held at Williamsburg, Virginia, January 17-23, 1960, and is published in the Reviews of Modern Physics (ref. 1). Although primary emphasis will be given here to material not contained in that article, some repetition will be made in order to aid the continuity of this paper.

SYMBOLS

B	magnetic induction
c	half length of electrodes
d	depth of channel
E	electric field intensity
$F(\lambda,k)$	elliptic integral of first kind
H	total pressure head, $p + \frac{1}{2}\rho U^2$
i	$\sqrt{-1}$
J	electric current density
k	modulus of elliptic integral
k'	complementary modulus of elliptic integral, $\sqrt{1-k^2}$
K	complete elliptic integral, $F\left(\frac{\pi}{2}, k\right)$
K'	associated complete elliptic integral, $F\left(\frac{\pi}{2}, k'\right)$
l	half length of magnetic field

electrodes and the beginning
back onto the horizontal or x_1 axis. The symbol F() denotes the incomplete elliptic integral of the first kind and expresses a Schwarz-Christoffel transformation (see

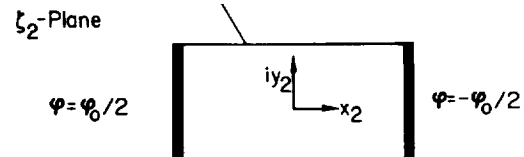

M Hartmann number, $\sqrt{\frac{\sigma B^2 \delta^2}{\eta}}$

p static pressure

$$\zeta_2 = F(\sin^{-1}\zeta_1, k) = \int_0^{\zeta_1} \frac{dw}{\sqrt{(1-w^2)(1-k^2w^2)}} = x_2 + iy_2 \qquad (1)$$

where w is a dummy variable of integration. The transformation given by equation (1) folds the walls and electrodes into the rectangle shown in the lower part of sketch (b). The potential distribution for this rectangular boundary is simply a linear drop between the two electrodes with no current flowing in the iy_2 direction. The desired solution[1] is then given by the complex potential function

$$\Phi = \varphi + i\psi = \frac{\varphi_o}{2K} F\left(\frac{i\zeta\pi}{2\delta}, k\right) \qquad (2)$$

where

$$\varphi = \frac{\varphi_o}{2K} \operatorname{Re} F\left(\frac{i\zeta\pi}{2\delta}, k\right) = \frac{\varphi_o}{2K} F(\alpha, k) \qquad (3)$$

$$\psi = \frac{\varphi_o}{2K} \operatorname{Im} F\left(\frac{i\zeta\pi}{2\delta}, k\right) = \frac{\varphi_o}{2K} F(\beta, k') \qquad (4)$$

The function K is the complete elliptic integral of the first kind and the quantities k, k', α, and β are determined by the relationships

$$k = \frac{1}{\cosh(c\pi/2\delta)}$$

$$k' = \sqrt{1 - k^2}$$

$$-\sin\frac{y\pi}{2\delta}\cosh\frac{x\pi}{2\delta} = \frac{\sin\alpha\sqrt{1 - k'^2\sin^2\beta}}{\cos^2\beta + k^2\sin^2\alpha\sin^2\beta} \qquad (5a)$$

[1] An alternate derivation that may be used to find the complex potential is to transform first with respect to $w_1 = e^{\zeta\pi/2\delta}$ and then with respect to $w_2 = F(\sin^{-1}w_1, k)$. A different but equivalent result for equation (2) is then found as

$$\Phi = \frac{\varphi_o}{2K} F\left[\sin^{-1}e^{\frac{\pi}{2\delta}(\zeta+c+i\delta)}, e^{-\frac{c\pi}{\delta}}\right]$$

where

$$\cos \frac{y\pi}{2\delta} \sinh \frac{x\pi}{2\delta} = \frac{\cos \alpha \cos \beta \sin \beta \sqrt{1 - k^2 \sin^2 \alpha}}{\cos^2 \beta + k^2 \sin^2 \alpha \sin^2 \beta} \tag{5b}$$

The rate of efflux of electricity from the electrodes at each point along their surface is found as

$$q(x) = i\sigma \left. \frac{d\Phi}{d\zeta} \right|_{y=\delta} = \sigma E_y(x,\delta) , \qquad |x| \leq c$$

$$= \frac{\sigma \pi \varphi_o}{4\delta K} \frac{1}{\sqrt{1 - \left[\frac{\cosh(x\pi/2\delta)}{\cosh(c\pi/2\delta)}\right]^2}} , \qquad |x| \leq c \tag{6}$$

Since the electric potential on the electrodes is a constant, no current flows along the surface of the electrodes in the stream direction. Equation (6) then represents the strength of the electric source distribution on the electrodes.

The solution for the electric field, equation (2), is verified in this paragraph by comparing its form at the limit where the electrodes either are very long or are points with the known solutions at these limits. It is found that equation (2) does reduce to the correct form when c/δ is taken to the limit, ∞ or 0. In the first case, when the length of the electrodes is allowed to grow without limit, so that $k \to 0$, the complex potential becomes

$$\Phi_{c \to \infty} = \frac{\varphi_o}{2K} F\left(\frac{i\zeta\pi}{2\delta}, 0\right)$$

From reference 2, the result is found as

$$\Phi_{c \to \infty} = \frac{i\varphi_o \zeta}{2\delta} \tag{7}$$

At the other extreme, when the length of the electrodes is reduced to zero while the total efflux of electric current is held equal to a constant $q = \varphi_o K'/K$, equation (2) reduces to a result that is in agreement with a relation that can be derived from an expression for a source cascade given by Lamb (see p. 71 of ref. 3); that is, when the quantities, $c \to 0$ and $k = 1/\cosh(c\pi/2\delta) \to 1$ in the complex potential, the various functions become

$$\zeta_2 = \int_0^{\zeta_1} \frac{dw}{1 - w^2} = \frac{1}{2} \ln \frac{1 + \zeta_1}{1 - \zeta_1}$$

and

$$\Phi = \frac{q\zeta_2}{\pi}$$

$$= \frac{q}{\pi} \ln \frac{1 + i \sinh(i\zeta\pi/2\delta)}{1 - i \sinh(i\zeta\pi/2\delta)} \tag{8}$$

If real and imaginary parts are taken, the electric potential and current functions for point electrodes are found as

$$\varphi = \frac{q}{2\pi} \ln \frac{\sin^2(y\pi/2\delta) + \sinh^2(x\pi/2\delta)}{4[\sinh^2(x\pi/2\delta)\sin^2(y\pi/2\delta) + \cosh^2(x\pi/2\delta)\cos^2(y\pi/2\delta)]} \tag{9a}$$

$$\psi = \frac{q}{\pi} \tan^{-1} \left[\frac{-\sinh(x\pi/2\delta)}{\sin(y\pi/2\delta)}\right] \tag{9b}$$

A 2 7 6

Equipotential and current lines computed by means of equations (3), (4), and (5) are shown in figure 2 for several values of the ratio of the length of the electrodes to the width of the channel, c/δ.

In practice, the infinite current density at the ends of the electrodes will only be approximated by a high but not infinite current. In order to see if the over-all potential would be affected an appreciable amount, the theoretical values are compared with measured values in figure 3 for an electrode length to channel width ratio of 2:1 as found on a resistance paper analog. The experimental points are seen to be in good agreement with the theoretical curves.

In the present experiment, the ratio of the electrode length to the channel width was chosen as 1:1. Since details of the electric field for this configuration contribute to some of the fluid motions observed, the electric field intensities, E_x and E_y, in the x and y directions are plotted in figure 4 on a sheared coordinate system in order to present the nature of the two-dimensional current distribution. The infinite current density at the ends of the electrodes, the symmetry of E_y, and the antisymmetry of E_x about the y axis are illustrated. The field distributions are not shown for the -y half plane. It is known, however, that the field quantities in the +y and -y half planes are mirror images of each other.

Magnetic Field

In order to complete the information needed for a theoretical analysis of the fluid motion, it is necessary to procure expressions for the magnetic field strength variation in the region occupied by the channel.

A theoretical prediction of the magnetic fields produced by the various iron-core shapes was felt to be too involved. Therefore, measurements taken of the magnetic field generated by the several magnet shapes are used instead.

Pressure Head Imparted by Pump

An estimate of the momentum increase given to the liquid by the pump is obtained by integrating the differential equations for the fluid along a streamline. For steady flow, the equations may be written as

Ohm's law:

$$\vec{J} = \sigma(\vec{E} + \vec{U} \times \vec{B}) \tag{10}$$

Momentum equation:

$$\rho(\vec{U}\cdot\vec{\nabla})\vec{U} + \vec{\nabla}p = \eta\nabla^2\vec{U} + \vec{J} \times \vec{B} \tag{11}$$

Continuity:

$$\vec{\nabla}\cdot\vec{U} = 0 \tag{12}$$

Maxwell's equations:

$$\vec{\nabla}\cdot\vec{B} = 0 \tag{13}$$

$$\vec{\nabla}\cdot\vec{E} = 0 \tag{14}$$

$$\mu\vec{J} = \text{curl } \vec{B} \tag{15}$$

where μ is the magnetic permeability and η is the viscosity. The vorticity in the fluid is given by

$$\vec{\Gamma} = \frac{1}{2} \text{curl } \vec{U} \tag{16}$$

and the total pressure head by

$$H = p + \rho \frac{U^2}{2} \tag{17}$$

If equations (10), (12), (16), and (17) are introduced into equation (11) and the fluid motion is assumed to be two-dimensional, the following expressions are obtained for the variation of H as the fluid passes through the electromagnetic fields

$$\frac{\partial H}{\partial x} - 2\rho v\omega = \sigma B_z(E_y - uB_z) + \eta\nabla^2 u \tag{18a}$$

$$\frac{\partial H}{\partial y} + 2\rho u\omega = -\sigma B_z(E_x + vB_z) + \eta\nabla^2 v$$

where

$$\omega = \frac{1}{2}\left(\frac{\partial v}{\partial x} - \frac{\partial u}{\partial y}\right)$$

is the z component of the vorticity vector $\vec{\Gamma}$.

The terms uB_z and vB_z express the electric potential developed by the motion of the fluid through the magnetic field and are referred to as the back or counter emf, because they oppose the emf impressed across the pump by an external source. The magnetic field strength, B_z, consists of a combination of the field imposed by the electromagnet and of the field generated by the electric currents flowing in the fluid. An estimate of the magnitude of this induced field can be obtained from the relation

$$\vec{A} = \frac{\mu}{4\pi}\iiint_V \frac{\vec{J}\,dv}{r} \qquad (19)$$

where $\vec{A}$ is the magnetic vector potential defined as curl $\vec{A} = \vec{B}$ with $r = \sqrt{(x - x')^2 + (y - y')^2 + (z - z')^2}$ and V as the volume in which the electric currents, $\vec{J}$ (see eq. (10)), are flowing. As mentioned previously, in the experiments to be considered, both the back emf and the secondary magnetic field given by equation (19) are at least 10^{-3} times smaller than the imposed electric and magnetic fields and they may therefore be ignored in the present analysis.

Equation (18a) can be simplified further by dropping the term $2\rho v\omega$ which is small in view of the fact that the cross-stream velocity is generally near zero and the vorticity, ω, is not large. Similarly, the viscous effects are small over the short distance occupied by the electromagnetic fields, so that the terms $\nabla^2 u$ and $\nabla^2 v$ can be deleted from equation (18a). If the relation $\sigma E_y = -\partial\psi/\partial x$ is used and the terms just discussed are dropped, equation (18a) may be written as

$$\frac{\partial H}{\partial x} = -B_z \frac{\partial \psi}{\partial x} \qquad (20a)$$

Similarly, equation (18b) reduces to

$$\frac{\partial H}{\partial y} + 2\rho u\omega = -B_z \frac{\partial \psi}{\partial y} \qquad (20b)$$

Since the cross velocity, v, is small, the streamlines will lie nearly along y = constant lines so that the integration of equation (20a) can be carried out to yield

$$H(x,y) - H_\infty(y) = \sigma \int_{-\infty}^{x} B_z E_y dx \qquad (21)$$

where $H_\infty(y)$, the pressure head upstream of the pump, may be a function of the cross-stream distance, y, if the viscous boundary layer is sufficiently developed. The pressure head $H(x,y)$ in equation (21) is assumed to be a function of only x and y within the electromagnetic field region. Downstream of the electromagnetic fields, however, it is a function of only y if viscous forces are assumed to be negligible. In both of these regions, the vorticity ω can be computed from equation (20b).

In the discussion to follow, it is convenient to simplify equation (21) by assuming that the magnetic field strength B_z is of constant strength in the region covered by the plan form of the iron core of the magnet and zero elsewhere.[2] The values for the extremities of the magnetic field, $\pm l$, correspond then to the edges of the iron core. Equation (21) can then be written as

$$H(y) - H_\infty \approx B_z[\psi(-l) - \psi(+l)] = B_z \Delta\psi \qquad (22)$$

The quantities $\psi(-l)$ and $\psi(+l)$ are the values of the electric current stream function at the assumed upstream and downstream edges of the magnetic field and $\Delta\psi$ is the total current flowing in the magnetic field. These quantities may be determined from equation (4) or figure 2.

EQUIPMENT

Figure 1 presents a schematic diagram of the test arrangement used for the experiments. Various components of this equipment were chosen so that the motion of the fluid could be observed visually. In the vertical position shown for the channel, the copper sulphate salt solution (see appendix B) circulates through the test portion of the clear plastic channel (1 by 3-1/2 inches in cross section) from the bottom to the top reservoir. (For convenience of presentation, the photographs of the ink

[2]Inasmuch as the air gap between the magnet pole pieces is generally kept small in comparison with the width of the iron core in order to produce a strong field, it is also conducive to containing the magnetic field in this region. It can then often be assumed that the magnetic field is constant in the air gap between the pole pieces and zero elsewhere so that the area covered by the field is the same as the cross section or plan form of the iron core.

filaments to be presented in the succeeding figures will show the channel in a horizontal position with the fluid flowing from left to right.) Fluid in the upper reservoir returns to the lower reservoir by means of the second channel shown in figure 1 so that the same fluid (about 2-1/4 gallons) can be circulated continuously. Antiturbulence screens and a contraction section in the lower reservoir produce a uniform laminar stream at the entrance (or bottom) of the test channel. Most of the tests were conducted with the back side of the channel pushed against the rear pole face as shown in sketch (c) for convenience in alining the channel accurately. Only in one test was a small but detectable flow disturbance observed to be caused by the fact that the channel centerplane was 1/8 inch from the centerplane of the magnetic field. This case will be discussed in the section on test results.

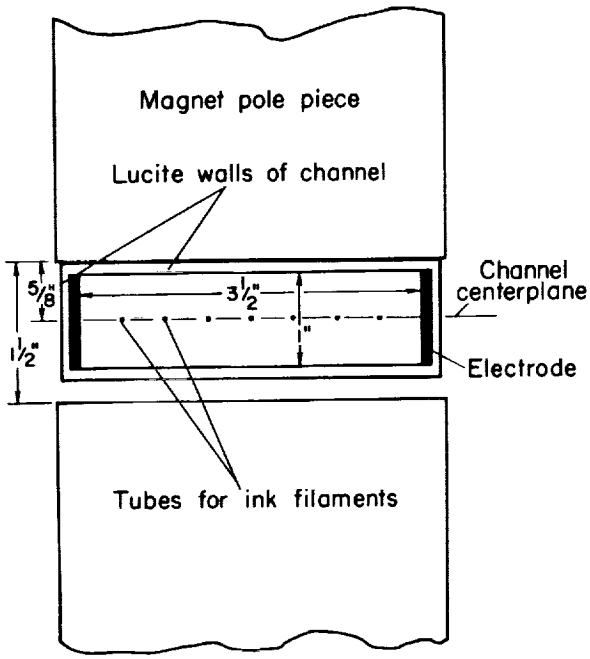

Sketch (c)

Since both the fluid and channel walls are transparent, it was necessary to inject ink into the stream to identify particular fluid elements. Seven ink tubes were located on the channel centerplane at the entrance to the test channel (sketch (c) and fig. 1) and fed by gravity pressure from an elevated reservoir. A hand operated cam served to cut off and regulate the rate at which ink was fed into the stream. Since the fluid and ink densities were closely matched (specific gravity = 1.040 ±0.001), the shape and length of the filaments remained nearly constant throughout the test section. The time-distance history of the various sets of ink filaments was recorded by a camera set to take one picture per second automatically. Location of these filaments in the photographs is aided by means of a reference grid that is graduated in inches and fastened to the rear surface of the test channel. Once the velocity of the filaments is determined, the dynamic pressure $(1/2)\rho(u^2 + v^2)$ can be computed.

The pressure rise across the electromagnetic field region was measured with a two-fluid manometer (fig. 1). Since the density of the two fluids was nearly the same, the small difference in pressure between the 5-inch and 20-inch stations, where the pressure taps were located, resulted in about a 1-inch deflection of the manometer fluid interfaces. A reading accuracy of about ±0.002 inch made it possible to measure the rather small pressure differences (10^{-3} to 10^{-4} psi) to within an accuracy of several percent. This measurement of the static-pressure rise through the pump,

together with the determination of the velocity (and hence, dynamic pressure), yields experimental values for the local pressure head, $H = p + (1/2)\rho U^2$, of the stream. A correction for the fluid friction on the channel walls between the 5-inch and 20-inch stations was obtained by circulating the fluid through the test channel with another pump and recording the pressure drop that occurred at the various flow rates.

The electric field was impressed on the fluid by electrodes made of copper bus bar 3-1/2 inches long and energized by wet cell batteries capable of delivering several amperes at up to 24 volts. The electrodes extended over the full depth of the channel and were mounted flush with the inside of the channel walls. Most tests were carried out at 6, 12, and 24 volts (or 0.4, 0.8, and 1.60 amperes) impressed across the electrodes in order to see how the fluid motion would be affected by the amount of power applied.

A C-shaped iron-core magnet was used as the basic magnet on which the various modifications (fig. 5) could be added. Blocks of SAE 1020 steel were added to this basic 4- by 4-inch design in order to shape the magnet cross section and air gap according to rules to be developed in the next section. Results of a survey of the fields on the channel centerplane produced by the various shapes are shown in figures 6 and 7 for a current of 10 amperes through the windings. The field at the center of the air gap is shown in figure 8 for the range of currents available. Inaccuracies in these measurements do not exceed a probable error of about 50 gauss (i.e., about 1 percent).

A motor-generator set supplied the excitation current for this electromagnet. The voltage could be controlled to supply a current through the windings (1800 turns) at any desired value from about 2 to 15 amperes. A current of 10 amperes was chosen for the tests because the magnetization curves (fig. 8) tend to level off at about that value.

TEST RESULTS

In the previous sections, equations have been developed to provide an estimate of the momentum imparted to an electrically conducting fluid by electric and magnetic fields. The equipment used in the experiments has also been described. It is now possible to proceed with a description of the several tests carried out, to identify particular flow phenomena, and to associate them with the elements of the electric and magnetic fields which cause these various fluid motions.

Consider first the flow induced in the test channel by the fields of the 4- by 4-inch magnet and the 3-1/2-inch electrodes. Figure 9(b) presents a typical photograph of the locations of several sets of ink filaments that depict the motion of the fluid through the channel. Since each set of filaments is released simultaneously, a displacement between them indicates a velocity difference in the fluid near the filaments. A small velocity difference causes a sizeable streamwise separation if it prevails for an appreciable distance along the channel. For this reason, the ink profiles near the exit of the test channel amplify any variation in the velocity possessed by the stream as it leaves the region where the body forces are applied. Local values of the velocity are obtained from the slope of the time-distance history of the ends of the filaments.

The distance decrement shown in figure 9(b) for the center filaments expresses a velocity deficiency in the fluid flowing along the center of the channel. In order to determine what characteristics of the electromagnetic fields cause this velocity variation, a comparison is made in figure 9(a) of the 4- by 4-inch magnet plan form with the electric current pattern of the 3-1/2-inch electrodes. Since the ends of the magnet do not follow any particular current line but cross several of them, the momentum imparted to the fluid by $\vec{J} \times \vec{B}$ (see eq. (22)) on each streamline is a minimum at the center where the fringing or spreading out of the electric current lines is a maximum. Near the walls, all of the current interacts with the magnetic field to produce the highest momentum possible for that arrangement. Since the flow velocities across the channel are negligible ($v \approx 0$), the pressure gradient, $\partial p/\partial y$, across the channel is also negligible. Therefore, any variation in the streamwise momentum or pressure head, H, appears in the dynamic pressure or velocity of the fluid as exhibited by the filaments in figure 9(b). Sketch (d) presents the momentum increase as computed by equation (21) and equation (22) and as measured in the test channel. All of the data have been normalized to an assumed current of 1 ampere. The two curves obtained with equation (22) represent two assumed variations in the magnetic field. The first, $l = \pm 2$ inches, assumes that the magnetic field is constant (4800 gauss) and is confined to the air gap between the magnet pole pieces. The second field distribution, $l = \pm 2.75$ inches, is the approximate rectangular fit (see fig. 6(a)) to the measured data for the square magnet. Results obtained with equation (21) for the pressure head, also shown in sketch (d), are the most accurate of the three theoretical curves since measured values for

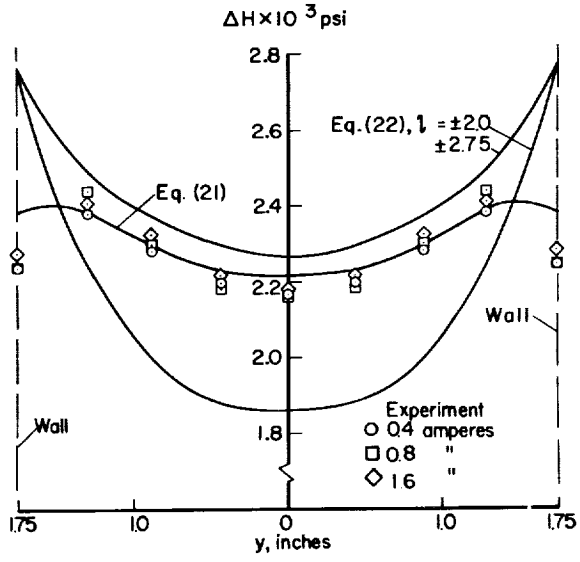

Sketch (d)

B_z were used in the integration of equation (21) for ΔH. Points shown in sketch (d) for the experimental data were determined from the measured values for the static pressure rise across the pump, the pressure drop due to fluid friction, and the local dynamic pressure variation expressed by the measured velocities on the centerplane of the channel.

The quantitative agreement of the experimental data with the theoretical curve shown in sketch (d) verifies the association made there between the velocity deficiency of the fluid near the center of the channel and the mismatch of the square shape of the magnet with the spreading out of the electric current lines.

The variation across the channel in the velocity (or pressure head) leads to vorticity that is introduced into the stream by the electromagnetic body force distribution. At low or nearly zero flow rate through the pump, this vorticity will roll up to form a vortex pair at the exit of the electromagnetic fields as shown in the upper part of figure 10(a). Fluid that is in the electromagnetic region, and hidden from view by the magnet pole pieces, also circulates in such a way as to form two more vortices. The relative strength and position of these four vortices depend on the applied power, flow rate, and viscous Reynolds number. Figure 10 was obtained by permitting fluid to circulate until ink filaments extended throughout the channel. The net flow was then stopped by a paddle and the picture taken as the filaments rolled up. The ink filament pattern shown in the lower part of figure 10 illustrates the streamline locations when the magnetic field has been designed to eliminate the circulation observed for the square magnet plan form. Details that lead to such a design are discussed in the next section.

Local values for the electric current components, E_x and E_y, induced in the fluid by the 3-1/2-inch electrodes are presented in figure 4. The body force distribution is related to E_x and E_y by the products, $\sigma E_x B_z$ and $\sigma E_y B_z$. In the ideal one-dimensional situation, E_x would be zero and E_y would be a constant. Although the distribution shown is quite nonuniform, none of the steady-state cases investigated here exhibited a measurable flow irregularity that was sustained outside of the pump and that could be traced to the peaks or valleys in the body force distribution. A particular streamline is deflected sideways about 1/8 inch by the high current densities at the ends of the electrodes, but it very nearly returns to its original path as it emerges from under the magnet.

One such disturbance does manifest itself in the unsteady case when the pump is turned on or off. It is caused by the nonuniform current densities at the ends of the electrodes (see fig. 4) and the resultant cross-stream variation of the pressure head at the ends of the magnetic field. Forward (+x) displacement of the fluid near the four ends of the electrodes as the fields are first applied causes sidewise motion of fluid a short distance from the center so that the ink lines buckle in the manner shown in figure 11. Such a streamline distortion occurs when

the magnet or electric field is turned on or off. This particular picture was taken a few seconds after the magnet was turned off while the fluid coasted to a stop. Eddy currents are induced in the fluid (and in the magnet core) by the rise or decay of the magnetic field, but the body forces[3] they induce appear not to be the cause of the streamline distortion shown in figure 11.

Magnet Plan Form Adapted to Electric Current Pattern

The previous discussion indicates that the choice of a square (or rectangular) magnet plan form is not in conformity with the electric current pattern of the 3-1/2-inch electrodes. In order to recover a uniform or one-dimensional stream, the magnet contour should then be shaped or adapted to fit the electric current pattern. Two magnet shapes that approximate the 90-percent ($\psi = \pm 0.45$) and the 98-percent ($\psi = \pm 0.49$) current lines are indicated in sketch (e) by the heavy lines. The plan

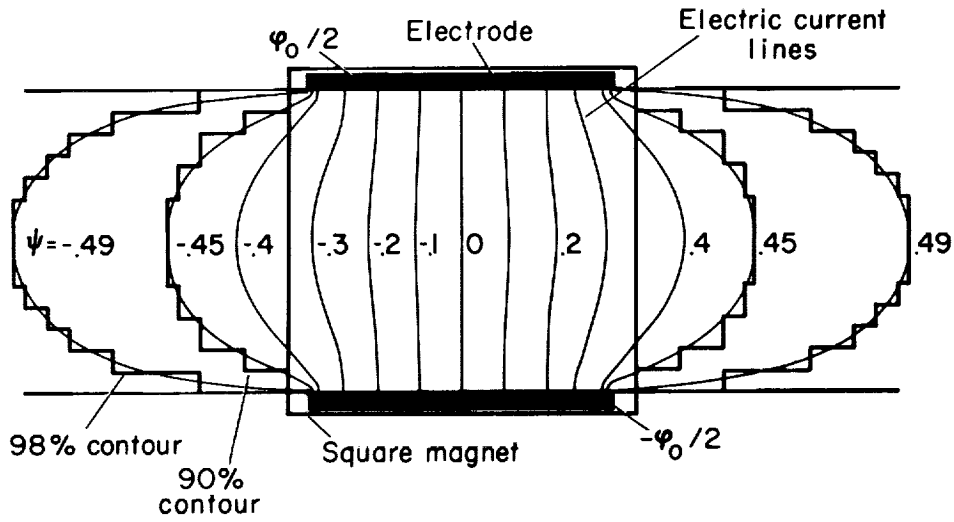

Sketch (e)

[3]Copper bars 1/8 by 1 by 4 inches held in the edge region of the magnet air gap will experience a small inward force when the magnet current is cut off abruptly. If a liquid metal were being pumped, it would then, because of its higher electrical conductivity, probably undergo motion not observed with the copper sulphate solution if the magnetic field strength changes rapidly.

form of the 4- by 4-inch magnet is also shown. Irregularities arise in these shapes from the edges of the iron plate stock used in constructing the pole-piece additions. No effort was made to round off the corners because they did not seem to affect significantly the strength of the magnetic field near the centerplane of the channel. The magnetic field strength B_z on the centerplane of the channel is presented in figures 6, 7, and 8 for these magnet plan forms. The 90-percent and 98-percent contours represent an attempt to produce fields which cover equal amounts of electric current on all streamlines so that, according to equation (22), the pressure head will be constant over the cross section of the stream at the exit of the region where the body forces are applied. Photographs of typical sets of ink filaments presented in figure 12 show a progressive change in the flow uniformity as predicted by equation (22). The velocity of the filaments nearest to the wall of the 90-percent contour is noted to be larger than those near the center. The small cross-stream variation in the velocity is attributable to the fact that about 10 percent of the electric current at the center of the channel is not covered by the magnet and therefore it is not effective in accelerating the fluid.

Cross-stream variations in the velocity are shown in figure 13(a) for a potential φ_o of 6, 12, and 24 volts (0.4, 0.8, and 1.6 amperes) applied to the electrodes. From these velocity curves and the pressure differences measured for those runs, a comparison is made in figure 13(b) of the variation in the theoretical and experimental total pressure head imparted to the fluid by the various contours for an assumed current of 1 ampere. The reduced flow rate experienced with the 98-percent contour is a result of a reduced magnetic field strength compared with the square magnet shape. Since the number of ampere turns is the same for all three magnets, the local field strength decreases with an increase in the plan-form area.

It is to be noted in figure 13(a) that at 6 volts the boundary layer on the side walls builds up enough in 15-20 inches to include the outer ink filaments. At 12 volts and 24 volts the Reynolds number is high enough (Re > 600) so that the boundary layer on the side walls does not enclose any filaments. In the plane perpendicular to the one being observed, the boundary layer develops fully in about 15 inches. If the boundary layer were ever to become fully developed so as to fill the entire channel, the ink filament at the center of the channel would be accelerated to a velocity 1.83 times the average velocity of the fluid in the channel.[4]

---

[4] The fully developed velocity distribution in a rectangular channel is given on page 197 of reference 4 as

$$u = \frac{1}{2} K \left[\delta^2 - y^2 + \frac{4}{\delta} \sum_{n=0}^{\infty} \frac{(-1)^{n+1}}{N^3} \operatorname{sech} \frac{Nd}{2} \cosh Nz \cos Ny \right]$$

where

$$N = \frac{(2n+1)\pi}{2\delta} \quad \text{and} \quad K \left(\frac{2}{3} d\delta^3 - \frac{8}{\delta} \sum_{n=0}^{\infty} N^{-5} \tanh \frac{Nd}{2} \right) = 2 d\delta U_{av}$$

The high degree to which the 98-percent contour matches the electric current pattern is borne out also in the lower part of figure 10 where the shape of the streamlines is shown when the flow rate has been reduced to zero. No change in the streamline pattern occurs even though the fluid was held stationary for a number of seconds. Under the same circumstances, the pump with a square magnet pole piece will induce two substantial vortices at the exit of the magnetic field region as shown in the upper part of figure 10 and some circulation under the pole pieces. Weak, diffuse vortices appear when the flow with a 90-percent contour is stopped with the hand paddle. It was in this case that the ink filaments did not stay on the channel centerplane but progressed in a corkscrew fashion in the z direction. No motion in the z direction occurs when the channel and air gap centerplanes are alined.

The unsteady flow case for both the 90-percent and 98-percent contours was also examined. With the 90-percent contour a pattern similar to that in figure 11 occurs, but the deflections or humps are much smaller as a result of the smaller pressure head deficiency at the center than for the square contour. No change in the streamline pattern is observed with the 98-percent magnet shape when the electromagnetic fields are turned on or off.

An additional flow phenomenon that was observed after several minutes of operation of the pump was a small and almost uniform velocity gradient across the channel. The cause of this gradient was traced to the electrode surfaces which begin to become contaminated in a nonuniform fashion after about 1 minute. In appendix B, it is shown that the condition of the electrode surfaces deteriorates with time at a rate that increases with the current density. Since the electric current density from the electrodes (see eq. (6)) is nonuniform, the contamination and the resultant interface resistance will vary along the electrode length. This variation will distort the electric field distribution from that predicted theoretically. The ends of the anode are affected first and bring about a reduction in the fringing of the electric field on that side of the channel. Near the anode then, a larger portion of the current is effective in accelerating the fluid than on the cathode side in keeping with the observed data. These difficulties are avoided by taking all the data within the first minute of operation before the anode contamination becomes appreciable.

Long Electrodes

As stated previously, most one-dimensional analyses assume that the electric and magnetic fields are uniform across and vary slowly or not at all along the channel. A completely uniform electric field can be procured by choosing the center portion of the field induced by electrodes which are long compared with the length of the magnetic field. The magnetic field of the 4- by 4-inch magnet is wide enough to produce a field uniform

across the channel. In this model then, only the center portion of the total electric current passing through the electrodes interacts with the magnetic field to accelerate the fluid, and the nonuniform electric current densities near the ends of the electrodes are well outside of the region of the magnetic field. The filaments shown in figure 14 illustrate the character of a stream propelled by such an arrangement; the electrodes are 16 inches long (electrode length/channel width = 4.57). End effects of the electrodes are eliminated as evidenced by the uniformity of the stream. Irregularities in the relative location of the ink filaments are believed to be caused by nonuniformities in the stream as it leaves the lower reservoir and enters the test channel. The velocity profile that exists in the fluid in front of the electromagnetic field region is not changed by the body forces so that it persists throughout the test channel. It can then be assumed that nonuniformities are not introduced into the stream by the force field. However, less than one-third of the current interacts with the magnetic field to increase the momentum of the stream.

Electric Current Barriers

Sizable changes can be brought about in the electric current pattern of a set of electrodes by placing insulators at various locations in the paths of the current. Such current barriers have been proposed as a means by which the electric current can be forced to flow more nearly straight across the channel rather than in large loops that extend upstream and downstream of the electrodes (see, e.g., ref. 5). Figure 15(a) illustrates the effect of two such barriers on the electric current lines for the 3-1/2-inch electrodes in the 1- by 3-1/2-inch channel. In principle, the ratio of electrode length to channel width is changed from 1:1 to 2:1 because the current distribution in the gap is the same as at the electrodes. A large number of these barriers would force the current to flow straight across so as to eliminate all the nonuniformities that arise from the finite length of the electrodes. In practice, however, only a limited number can be installed and their length will be finite. As part of the systematic study on the direct-current pump, test results obtained with the channel equipped with 3-1/2-inch electrodes, a square magnet, and two 11-inch barriers are presented in figure 15(b). The barriers are partially effective but a loss in momentum occurs at the center because the barriers are not infinitely long and thereby permit current to leak around the ends that are not under the magnet. An estimate of this current is obtained from a consideration of the length of the two current paths. Since the barriers are each 11 inches long and the channel is 3.5 inches wide, the ratio of the path length around the end of a barrier to that straight across is about $(25/3.5) \approx 7$. In the experiment, the total electric current and the current around the ends were measured as 0.77 and 0.1 ampere, respectively, or a ratio of $0.1/(0.77 - 0.1) \approx (1/7)$ in agreement with the predicted value. This 14-percent loss in current leads to an equal loss in pressure head at the center of the channel and to the velocity decrement demonstrated in figure 15(b).

Magnet Air Gap Adapted to Electric Current

An alternate method of producing a uniform stream with the square magnet and the 3-1/2-inch electrodes is acquired by satisfying equation (22) in a second way. It consists of an adjustment to the field strength rather than to the plan form of the magnet to fit the electric current pattern. In order to achieve this, the air gap is constructed so that the magnetic field strength B_z will compensate for the deficiencies in $\psi(l) - \psi(-l) = \Delta\psi$ along each streamline. Inserts for the square magnet were first determined by simple one-dimensional considerations in which it is assumed that the local magnetic field strength varies inversely with the local air gap. Coordinates for the air gap computed in this way are shown in sketch (f) as the values labeled first approximation. Results for such a magnet and the 3-1/2-inch electrodes are compared in figure 16 with the flow induced by a constant 1-1/2-inch air gap and already presented in figure 9(b). These air gap inserts cause the magnetic field to overcompensate at the center of the channel. The velocity profile has then an excess rather than a deficiency along the center line. Turbulence arises in the stream from the nonuniform pressure head in the output stream and from the vorticity generated by the curvature of the magnetic lines as they pass through the channel. Several trial and error modifications to the air gap size were then made to correct the first approximate design. A stream which has a uniform velocity is produced by the final model tested but turbulence is imparted to the stream by extraneous body forces which arise from the curvature of the magnetic lines of force. More satisfactory results could have been obtained by a combination of air gap inserts with magnet additions to contour the iron core cross section in order to achieve a desired velocity profile.

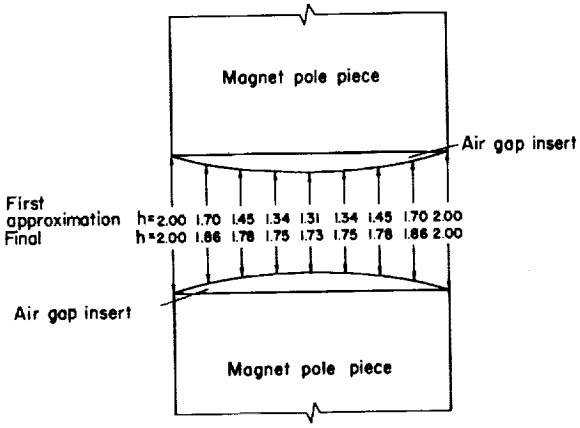

Sketch (f)

Three-Dimensional Fields

Two additional tests are described here to illustrate how the flow out of a pump is affected by components of the electromagnetic fields in a third direction. A cross-sectional view of each of the models studied and the resulting flow patterns are shown in figure 17. In both runs, 1/8-inch-thick iron plates are bolted to the pole faces in order to increase the magnetic field along the center line of the channel. The center portion of the electrodes is replaced by an insulator as shown

in figure 17(b) in an attempt to make the current flow as indicated. It was hoped that the current and magnetic lines would then intersect more nearly at 90° and the turbulence would be reduced. The low current density in the vicinity of the insulated portion of the electrodes appears to increase the turbulence so much as to offset any other advantages which may have been obtained by the curvature of the electric current lines. These examples illustrate that the flow out of the pump is sensitive to variations in the field strength in the third dimension. In the absence of an adequate theory to guide such a design, it is difficult to produce a satisfactory arrangement by these techniques.

CONCLUDING REMARKS

Results have been presented that illustrate the interaction of several configurations of electric and magnetic fields with an electrically conducting fluid in a channel. Certain flow peculiarities associated with these arrangements are identified with the characteristics of the electromagnetic fields which cause them. The approximate theory developed in the analysis predicts the total pressure head variations in the rectangular channel as accurately as could be determined experimentally. Other flow phenomenon, that was not considered here and not included in the final form of the equations developed in the analysis, will appear when gases and liquid metals are used as the medium to be accelerated under conditions in which the induced fields are comparable with the applied fields. Additional motions will occur in the fluid because of eddy currents that are induced by variations in the stream velocity. A number of variations and possibilities for the production of streams with certain characteristics could also be investigated. For example, consideration could be given to the possible advantages and effects which may occur when ideally curved shapes for the electrodes and for the channel walls are used in combination. It is of interest to note that it was possible to obtain a large variation in the velocity profile of the output stream in the rectangular channel tested here by a suitable choice in the form of the electric and magnetic fields.

Ames Research Center
National Aeronautics and Space Administration
Moffett Field, Calif., Aug. 24, 1960

APPENDIX A

RESUMÉ OF THE LITERATURE ON ELECTROMAGNETIC PUMPS

Although the electromagnetic device used in the present investigation is operated at a low power level compared to some liquid metal pumps, it is informative to consider the data available on and some of the difficulties encountered with the operation of electromagnetic pumps. The material in this section is drawn from papers by Cage (refs. 6 and 7), Barnes (ref. 5), Woollen (refs. 8 and 9), Watt (ref. 10), and Franco and Pedretti (ref. 11). Some of the power supply units which may be used to operate these pumps are described by Brill in reference 12. The units described in these articles cover a range of flow rates and sizes. The flow rate capacity varies from 1 to 10 gallons per minute for the small devices to several thousand gallons per minute for large pumps. These flow rates are sustained for a pressure difference across the electromagnetic field region of from several pounds per square inch to about 45 psi or 3 atmospheres. An electric current of several hundred amperes is used in the small units and over 20,000 amperes are used in the large pumps. The applied voltage is generally less than 2 volts. The largest current mentioned in the references cited here is that produced by a homopolar generator that is capable of supplying 200,000 amperes at 75 volts (see Brill, ref. 12).

The magnetic field strengths appear to be about 4000-6000 gauss and are generated by an electromagnet. The electric current used to drive the fluid is sometimes used to excite the magnet as a one or two turn coil. The low voltages remove the necessity for insulating materials which may be destroyed by the high operating temperatures of the fluid and pump. The operating efficiency is about 10 to 20 percent for the small pumps and 40 to 50 percent for the large pumps (see Barnes, ref. 5). These pumps are capable of operating at temperatures as low as the melting temperature of the fluid and up to about 1500° F.

If an alternating current power source is used to excite the magnet and to drive the fluid, eddy currents and nonsteady flow phenomena will arise in the fluid. The result is usually a less efficient operation than in the direct-current pump. Although power is more readily available for the a-c pump, the losses inherent in its operation may make its use uneconomical.

If the electrodes and the magnetic field extend along the channel for a number of channel widths, the flow will be one-dimensional because irregularities near the ends of the electromagnetic fields exert a negligible effect on the flow in comparison with the over-all impulse imparted to the fluid by the pump. The theoretical expressions for the velocity, pressure, etc., for the flow in such a channel have been found by Hartmann (ref. 13) when the fluid is viscous, incompressible and has constant

electrical conductivity. A number of complicating phenomena appear, however, when the length of the electrodes and of the magnetic field is about one channel width. The electric current, in this case, does not flow straight across the channel but a portion of it flows through fluid that is upstream or downstream (i.e., outside of) the magnetic field (see figure 9 so that a loss in the pressure head imparted to the fluid occurs in the vicinity of the center of the channel when the pressure head pumped against is near the maximum imparted to the liquid by the pump.

Several analyses have been carried out on the current contained in these fringe loops. Barnes (ref. 5) and Franco and Pedretti (ref. 11) discuss the fringe currents on a qualitative basis by use of an equivalent circuit that consists of resistances in parallel. In treating the problem of removing power from a hot gas stream, Sutton (ref. 14) and Fishman (ref. 15) derive an expression for the electric current distribution in order to compute the amount of current in the fringe field. The effect of several different longitudinal magnetic field distributions on the output of the device is investigated but the motion of the fluid is not considered. It is pointed out in these four references that the fringing of the magnetic field can also cause appreciable losses and nonuniformities in the stream if it extends much beyond the electrodes. Mention is also made of the fact that the eddy currents induced in the fluid by the overhanging magnetic field can cause turbulence and pressure losses. The amount of current flowing in the fringe loops of the electric field is increased by the so-called back or counter emf generated by the motion of the fluid through the magnetic field. Since the current flowing through the fluid in the magnetic field is opposed by the back emf and the current in the fringe loops is not opposed, the net result will be that a larger percentage of the total current will flow outside of the magnetic field region.

A nonuniformity arises in the imposed magnetic field as a result of the secondary magnetic field generated by the electric current flowing through the fluid. The increased field at the entrance to the pump and the decreased field at the exit can be largely compensated for (refs. 5 and 12) by either tapering the pole faces or by bringing an electric current lead from an electrode back across the top (or bottom) of the channel in order to generate a magnetic field opposite to the one generated by the current through the fluid. While both methods offer only partial compensation, the folded current configuration is a better approximation over a much wider range of electric current. It has the disadvantage that the space required for the current lead increases the air gap of the magnet and, therefore, the power required to produce a given field strength is also increased.

APPENDIX B

DEVELOPMENT OF COPPER SULPHATE SOLUTION

The requirements of the medium to be used in the present investigation are that it be transparent and of uniform density and electrical conductivity, that it should not change radically as a result of transmission of an electric current, or give off gas at the electrodes. It would be preferable that the medium did not give off toxic or poisonous vapors. Since liquid metals are opaque, one is forced to turn to salt solutions in which the current carriers are ions rather than electrons. In so doing, an electroplating process occurs at the electrodes whereby the passage of an electric current causes the anode to lose, and the cathode to gain, metal.

Some preliminary experiments were carried out with a sodium-chloride (NaCl) salt solution because it had a high electrical conductivity compared with other electrolytic solutions. Metal from the anode was taken into solution by the electric current and a sizeable quantity of gas was liberated at the electrodes. The gas caused a marked density variation in the fluid so that the electromagnetic effects were mixed with and often masked by the nonuniform properties of the solution. A copper sulphate solution ($CuSO_4$) with copper electrodes was then used for all subsequent tests because it is a nearly perfect plating solution and is easy to handle. No gas is emitted for potentials as high as 24 volts and the composition of the solution does not change perceptibly by the passage of the electric current. Some difficulty does arise in the current-voltage relationship as a result of the high current densities required to obtain a body force on the fluid that is large enough to support a satisfactory flow rate or pressure head. Theoretically, an infinite current density occurs at the ends of the electrodes (see eq. (6)), and so difficulty should be expected for the configuration being studied even for very small total currents through the pump. In order to minimize these variations with time, a series of tests were carried out with a uniform electric field in a rectangular box. The change in the electric current with time was due to some condition which develops at the surface of the electrodes (and not in the solution) after a certain amount of current has passed. A curve that illustrates the current as a function of time for a fixed voltage is shown in sketch (g) for a typical test. The starting, minimum, and final asymptotic values of the current were recorded for several values of the applied voltage

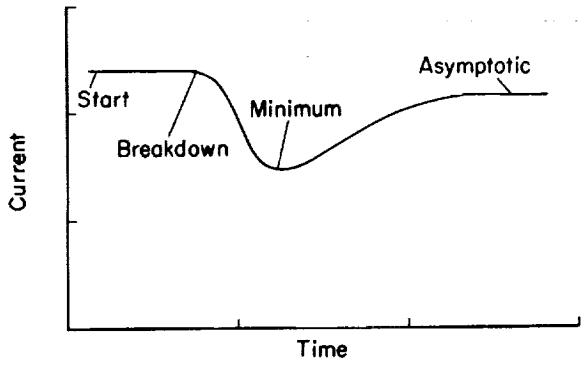

Sketch (g)

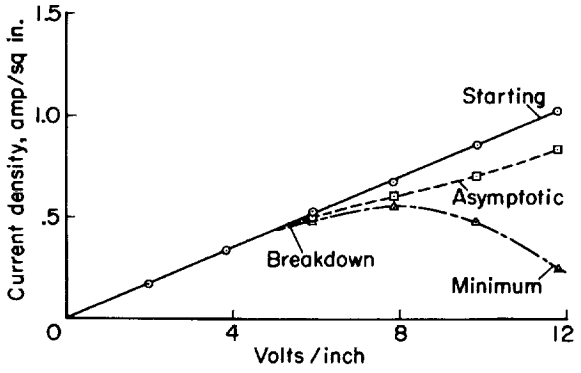

Sketch (h)

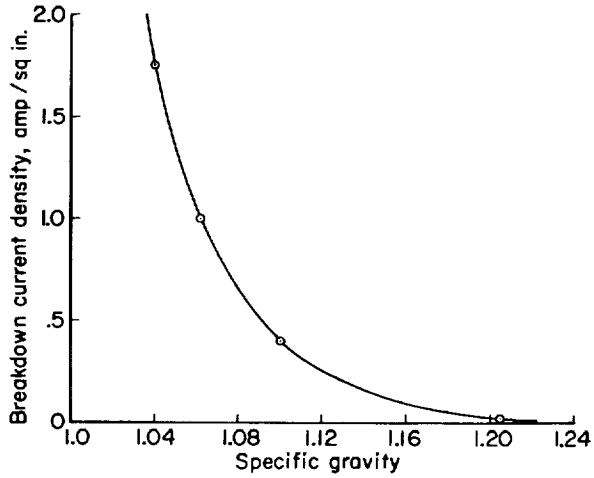

Sketch (i)

and specific gravity of the copper sulphate solution. Each test was started with freshly sanded electrodes and unused solution.[1] Sketch (h) illustrates the variation of the current with the applied voltage for a solution with a specific gravity of 1.100. The objective was to find the conditions which would yield the highest current density without an appreciable drop in the current. Also, the asymptotic curve should lie very near the starting curve. It was found that the more dilute solutions had the more desirable characteristics. Sketch (i) presents the current density (breakdown current) at which difficulty occurs at the surface of the electrodes as a function of the specific gravity of copper sulphate solutions. The conductivity of the solution is shown in sketch (j) as a function of the specific gravity. It becomes necessary to choose a solution with a specific gravity such that the conductivity is high enough to conduct enough current for the test without appreciable heating of the fluid and so that the breakdown current is as high as possible. Since these two requirements are in conflict, a solution with a specific gravity of 1.040 was chosen as an acceptable compromise for the present investigation. The initial and asymptotic current values do not differ by more than 1 or 2

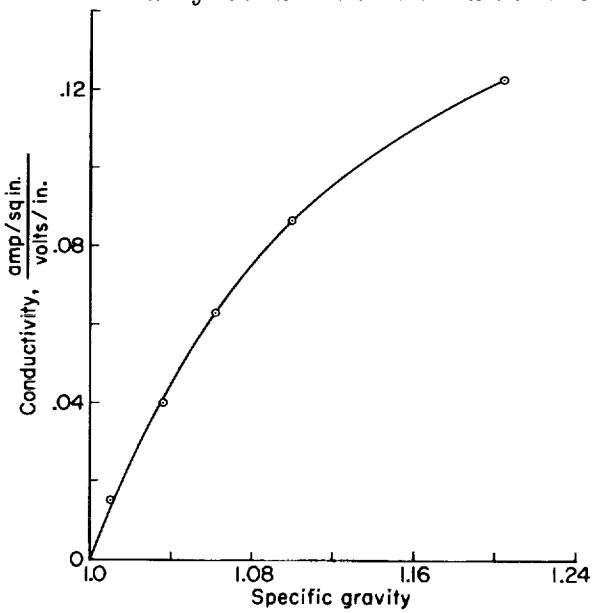

Sketch (j)

[1]Addition of even a small amount of sulphuric acid results in emission of gas at the current densities of interest in this paper. Therefore, acid was not added to the solution.

percent in such a solution. It was found that the electric current remained steady for a longer period of time when the solution was heated with activated charcoal and then filtered.

Several types and colors of ink were tried as filament indicators. It was found that the most suitable substance was any blue ink commonly used in fountain pens. The density was adjusted to correspond to that of the fluid (specific gravity = 1.040) by dissolving copper sulphate crystals in the ink. Ink filaments composed of such a combination did not diffuse enough to be objectionable throughout the test section of the channel. In turning the corners of the channel and passing through the screens the ink mixes readily with the copper sulphate solution so that distinct filaments are erased and repeated use can be made of a given batch of fluid. The ink causes a gradual darkening from light to dark blue but the solution remains transparent.

A few drops of liquid detergent were added to the solution in order to make the solution wet the walls of the channel and to prevent gas bubbles from clinging to the walls and screens.

REFERENCES

1. Rossow, Vernon J.: On Flow in Direct-Current Electromagnetic Pumps. Reviews of Modern Physics, vol. 32, no. 4, Oct. 1960.

2. Byrd, Paul F., and Friedmann, Morris D.: Handbook of Elliptic Integrals for Engineers and Physicists. Vol. LXVII of Grundlehren der Mathematischen Wissenschaften in Einzeldarstellungen. Springer-Verlag, Berlin, 1954.

3. Lamb, Horace: Hydrodynamics. Dover Pub., 1945.

4. Dryden, Hugh L., Murnaghan, Francis D., and Bateman, H.: Hydrodynamics. Dover Pub., 1956.

5. Barnes, A. H.: D-C Electromagnetic Pumps. Nuclear Reactor Experiments, J. Barton Hoag, ed., D. van Nostrand Co., Inc., 1958. pp. 272-279.

6. Cage, J. F., Jr.: Electromagnetic Pumps. Machine Design, vol. 25, no. 3, March 1953, pp. 178 ff.

7. Cage, J. F., Jr.: Electromagnetic Pumps for High Temperature Liquid Metal. Mechanical Engineering, vol. 75, no. 6, June 1953, pp. 467-471.

8. Woollen, W. B.: Electromagnetic Pumping of Liquid Metals. Fluid Handling, no. 62, March 1955, pp. 60-63.

9. Woollen, W. B.: Electromagnetic Pumping of Liquid Metals-II. Fluid Handling, no. 63, April 1955, pp. 90-92.

10. Watt, D. A.: Electromagnetic Pumps for Liquid Metals - Circulating Reactor Coolants and Fuels. Engineering, April 27, 1956, vol. 181, no. 4703, pp. 264-268.

11. Franco, Gianfranco, and Pedretti, Alberto: Pompe Elettromagnetiche. Tecnica Italiana, vol. 11, no. 7, Nov. 1956, pp. 481-490.

12. Brill, Edward F.: Development of Special Pumps for Liquid Metals. Mechanical Engineering, vol. 75, no. 5, May 1953, pp. 369-373.

13. Hartmann, Jul.: Hg-Dynamics I - Theory of the Laminar Flow of an Electrically Conductive Liquid in a Homogeneous Magnetic Field. Kgl. Danske Videnskabernes Selskab, Mathematisk-Fysiske Meddelelser, vol. 15, no. 6, Copenhagen, 1937.

14. Sutton, George W.: Electrical and Pressure Losses in a Magnetohydrodynamic Channel due to end Current Loops. General Electric Co., Aerosciences Lab. Rep. R59SD431, July 22, 1959.

15. Fishman, Frank: End Effects in Magnetohydrodynamic Channel Flow. Res. Rep. 78, AVCO Research Lab., June 1959.

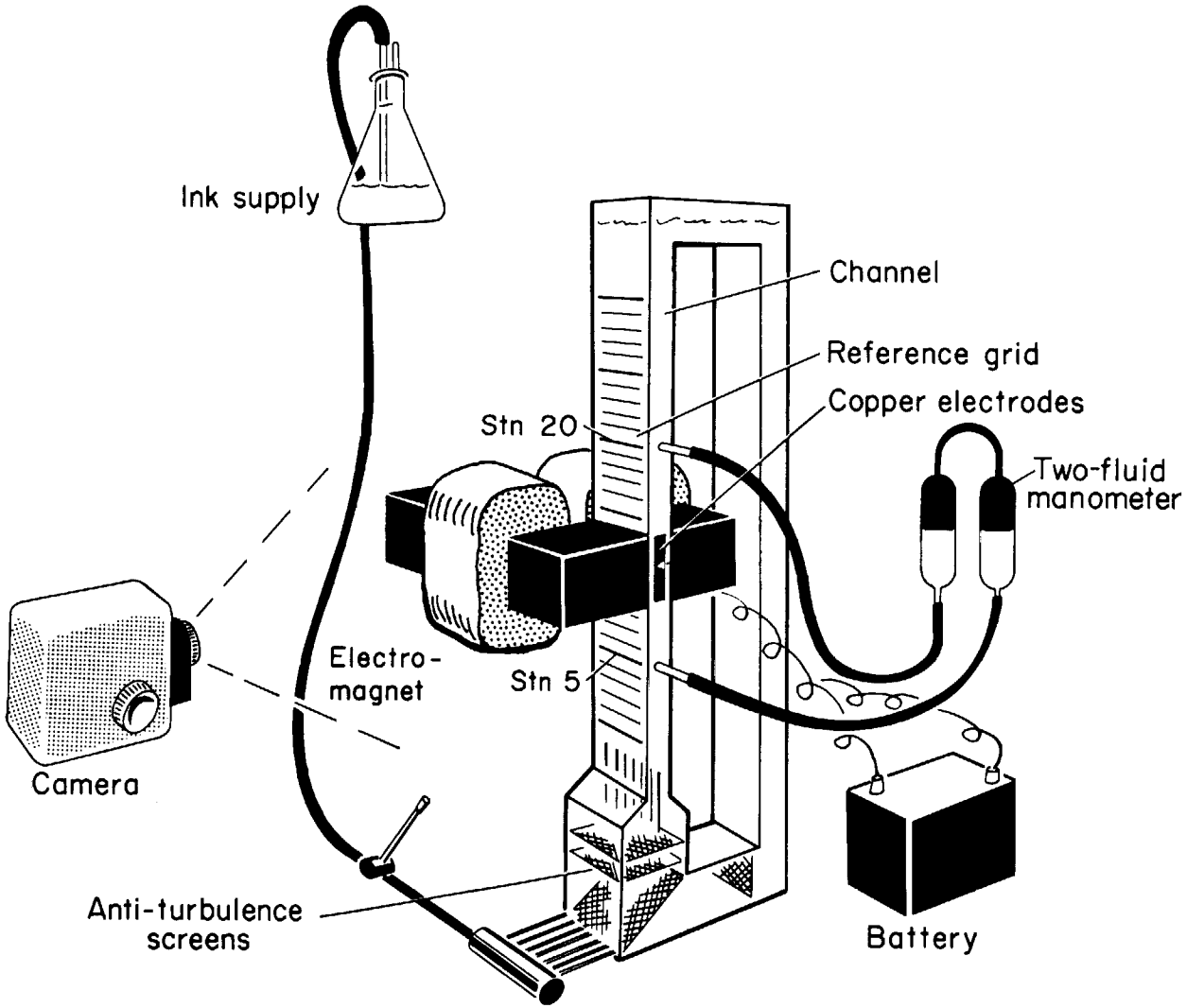

Figure 1.- Schematic drawing of test setup.

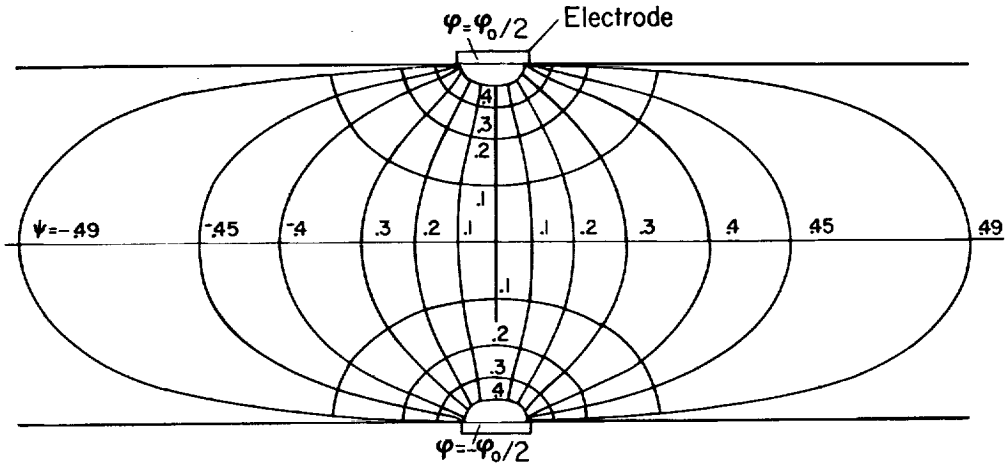

(a) Electrode length/channel width = 1/5.

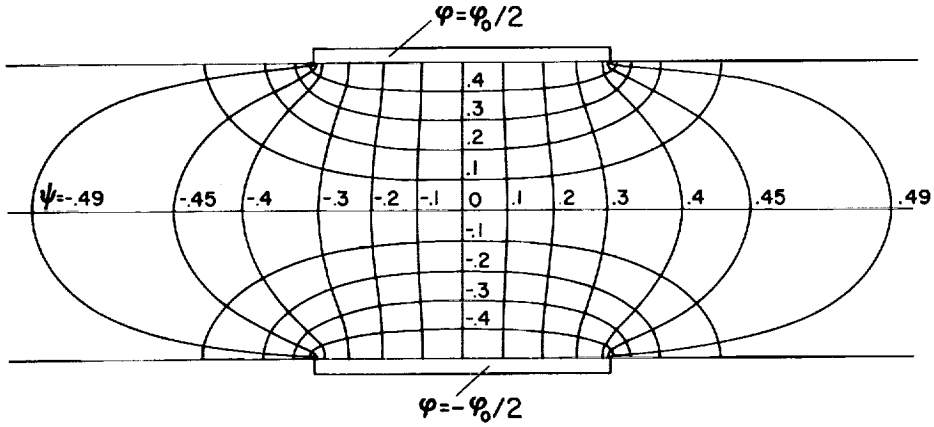

(b) Electrode length/channel width = 1/1.

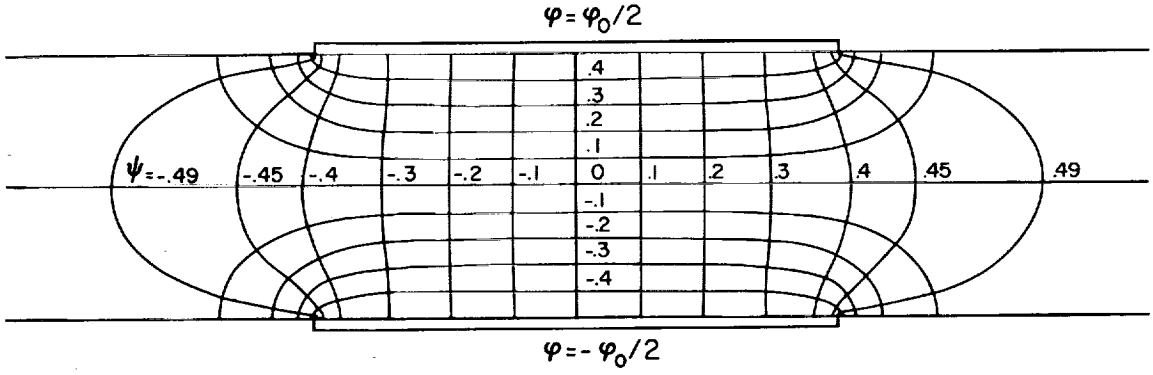

(c) Electrode length/channel width = 2/1.

Figure 2.- Equipotential and current lines in a two-dimensional channel.

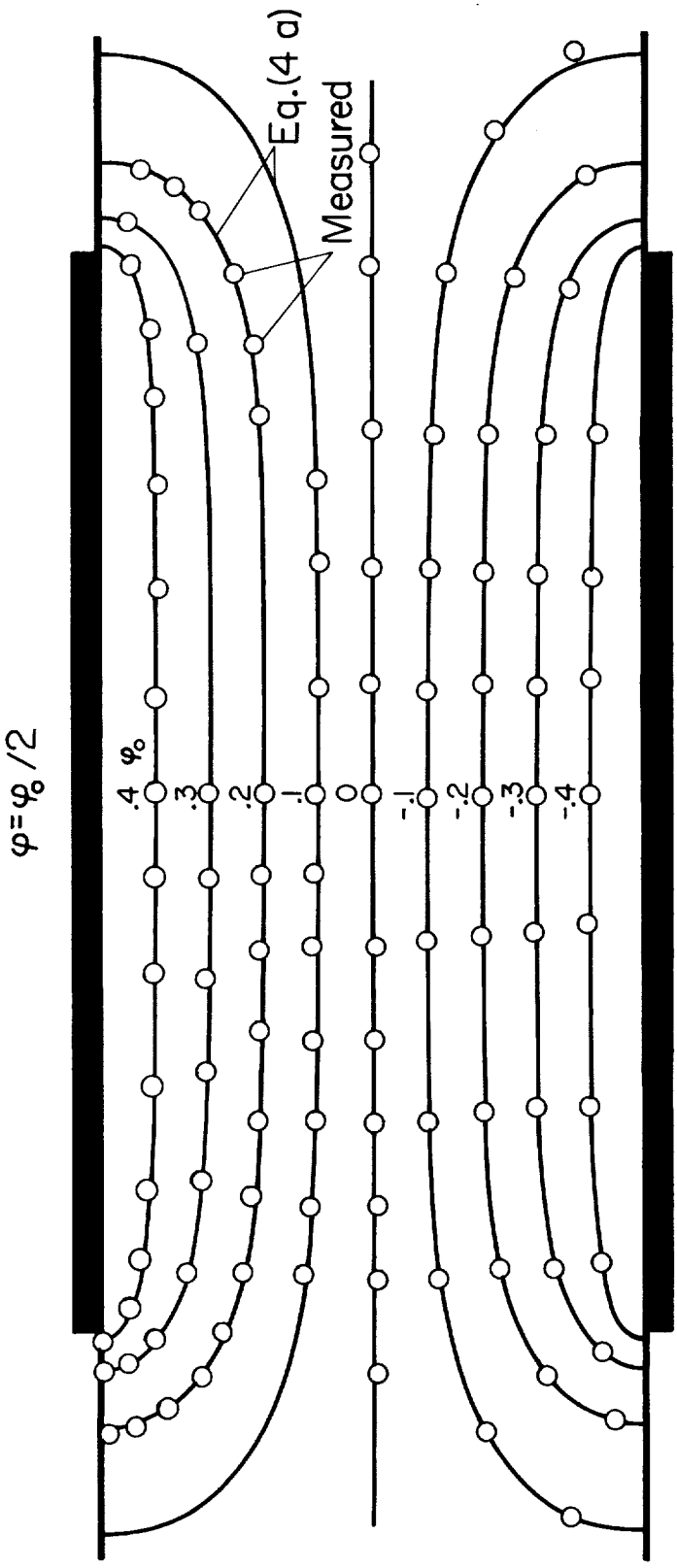

Figure 3.- Comparison of theoretical equipotential lines with experimental values obtained with resistance paper analog; electrode length/channel width = 2/1.

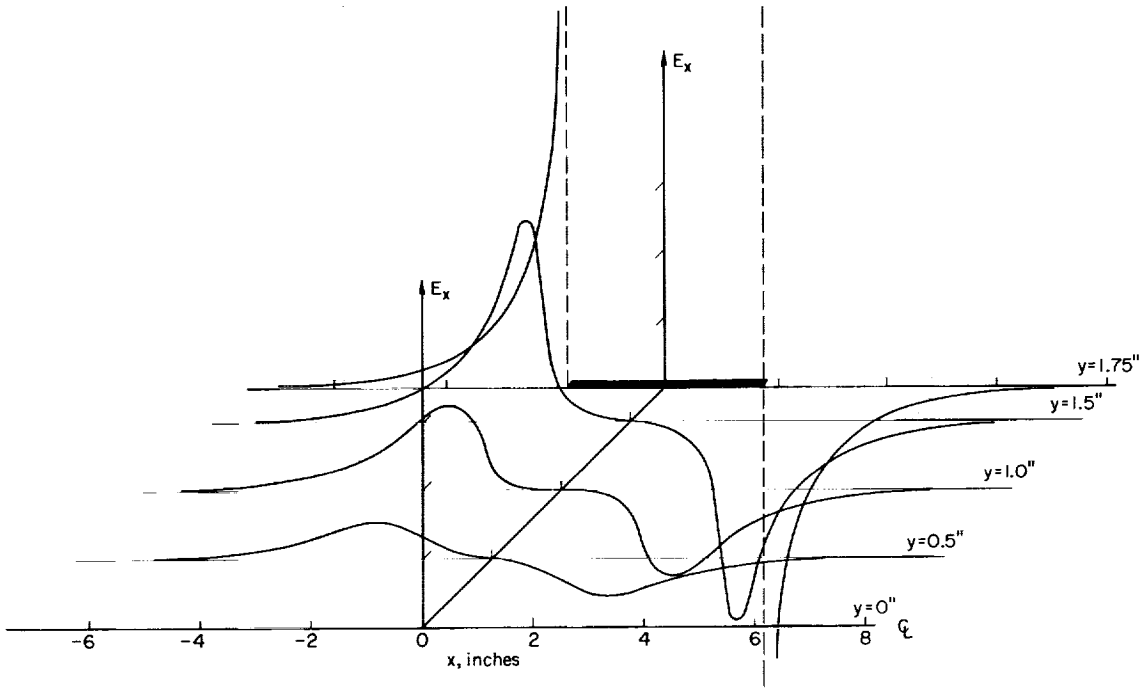

(a) Streamwise component, E_x.

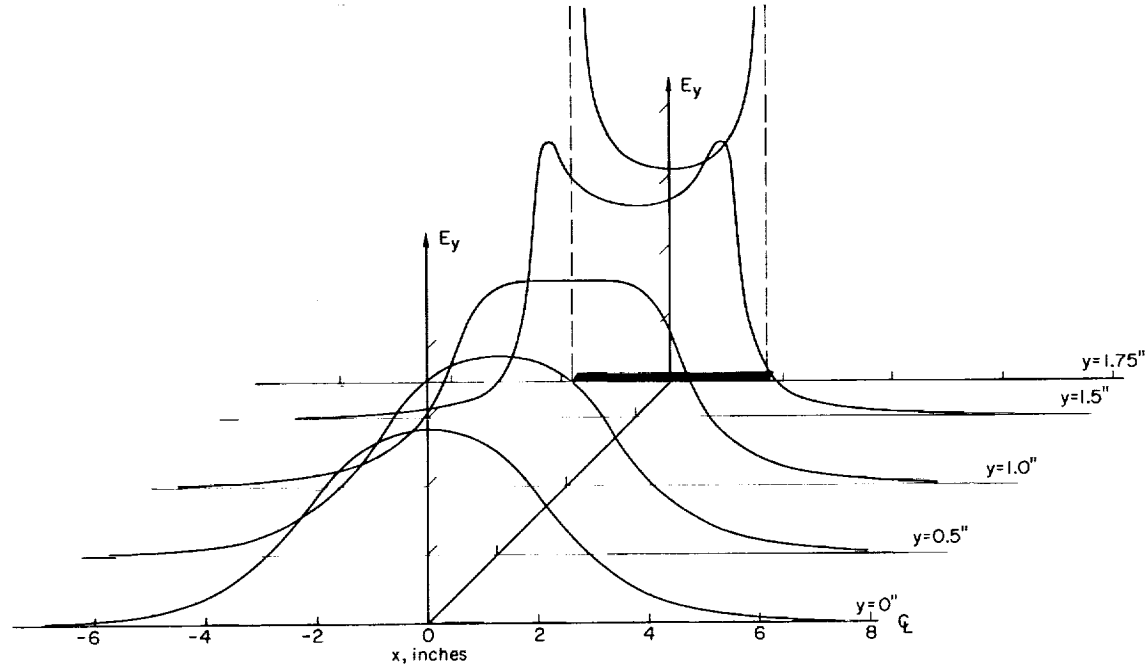

(b) Cross-stream component, E_y.

Figure 4.- Electric field intensity for electrode length/channel width = 1/1.

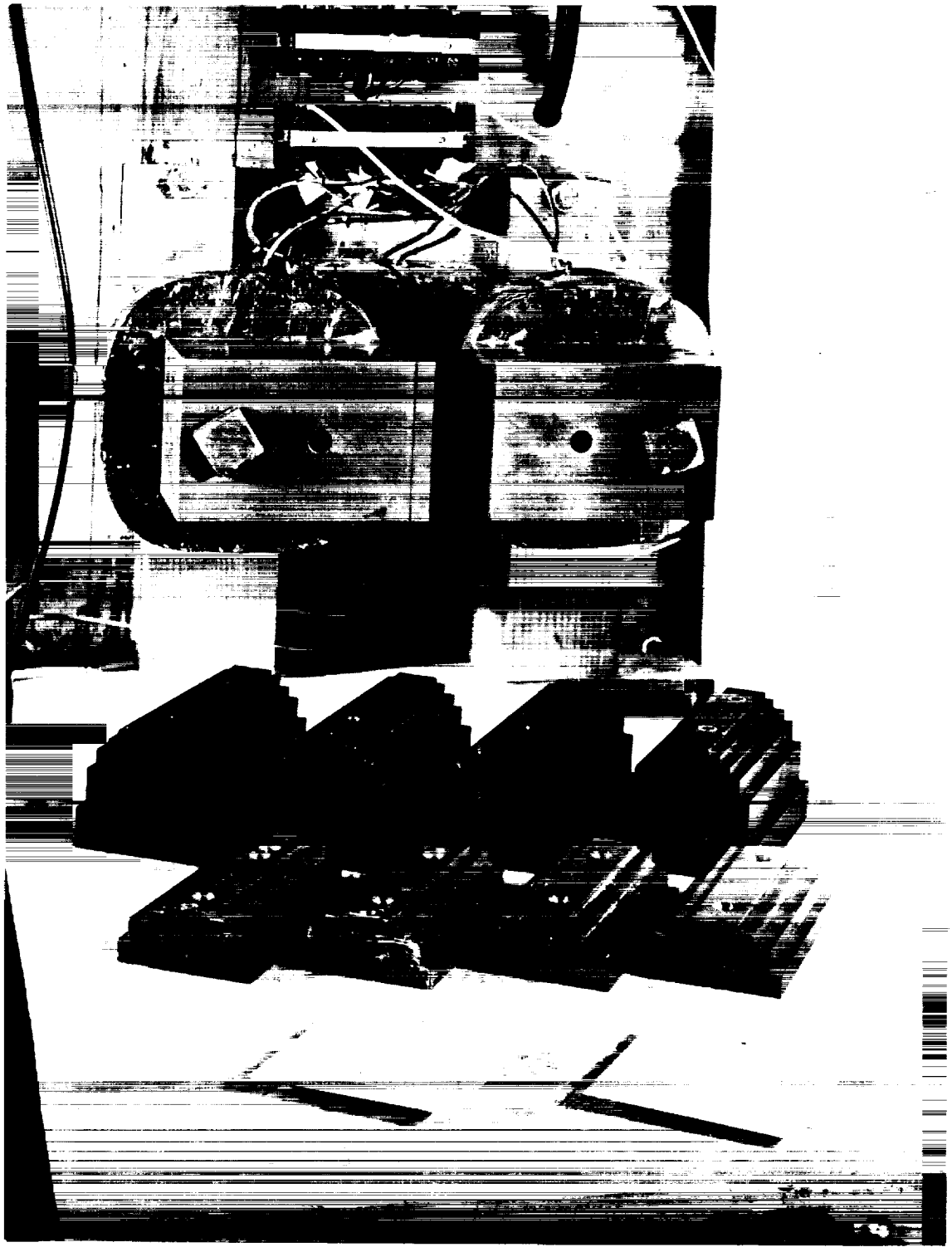

A-25990

Figure 5.- Electromagnet with 4- by 4-inch pole pieces and additions.

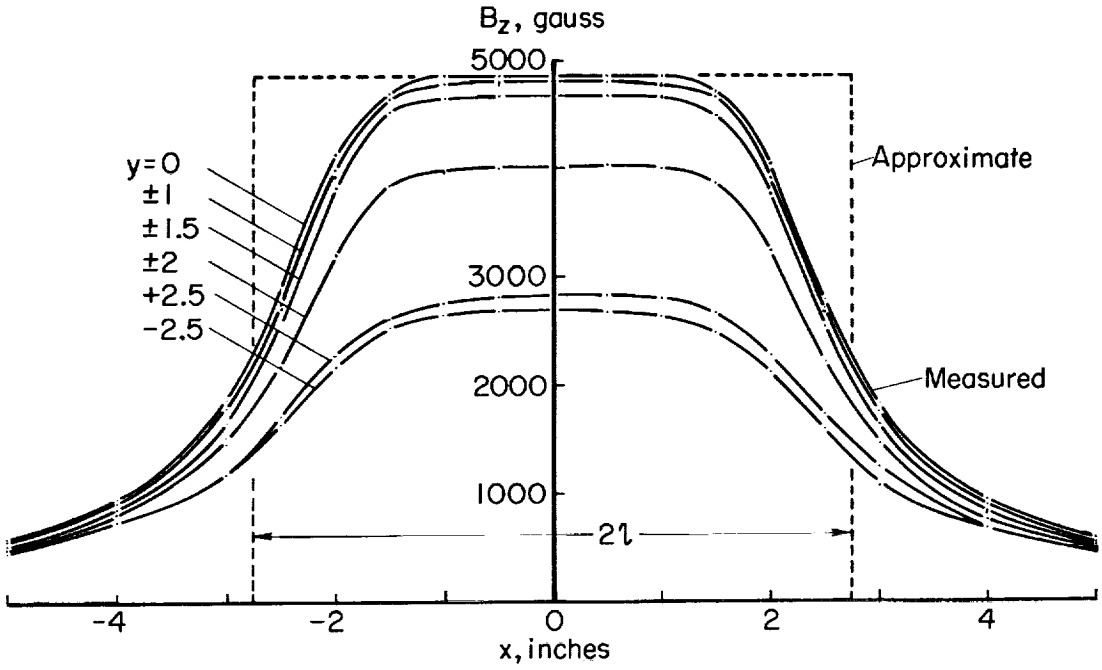

(a) Square pole pieces; 1-1/2-inch air gap.

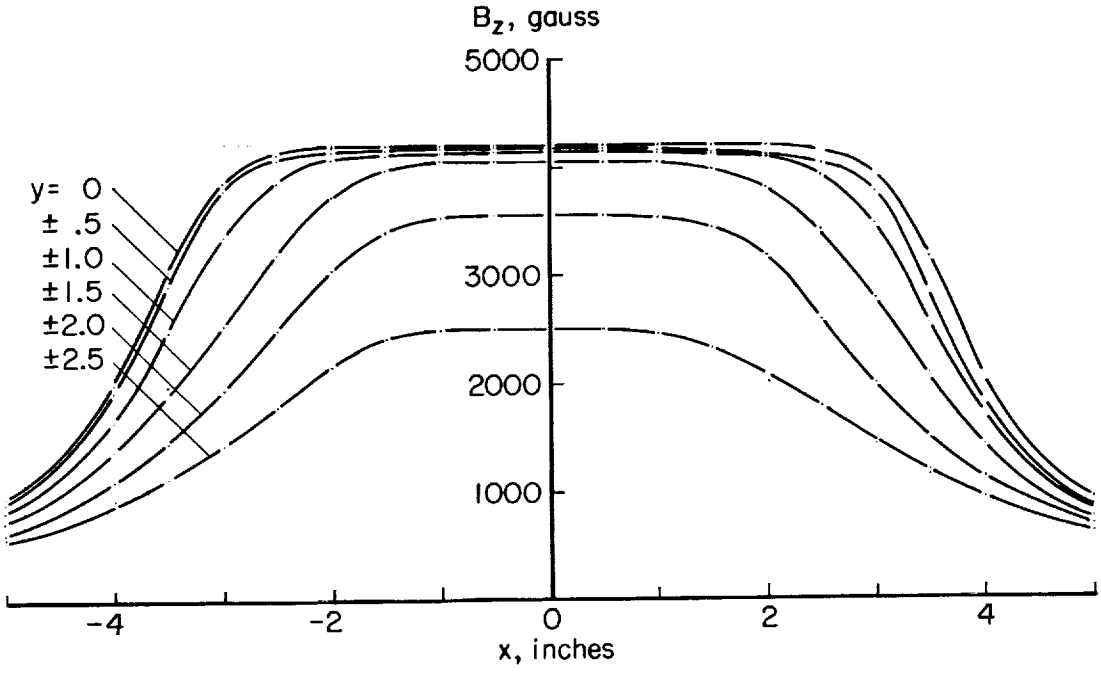

(b) 90 percent contour; 1-1/2-inch air gap.

Figure 6.- Magnetic field strength on centerplane of channel with 10 amperes through field windings.

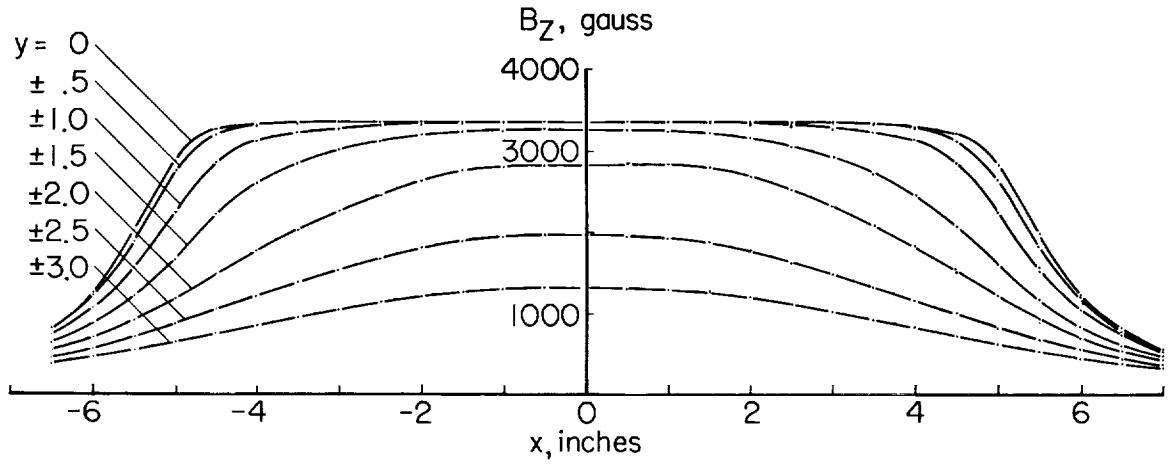

(c) 98 percent contour; 1-1/2-inch air gap.

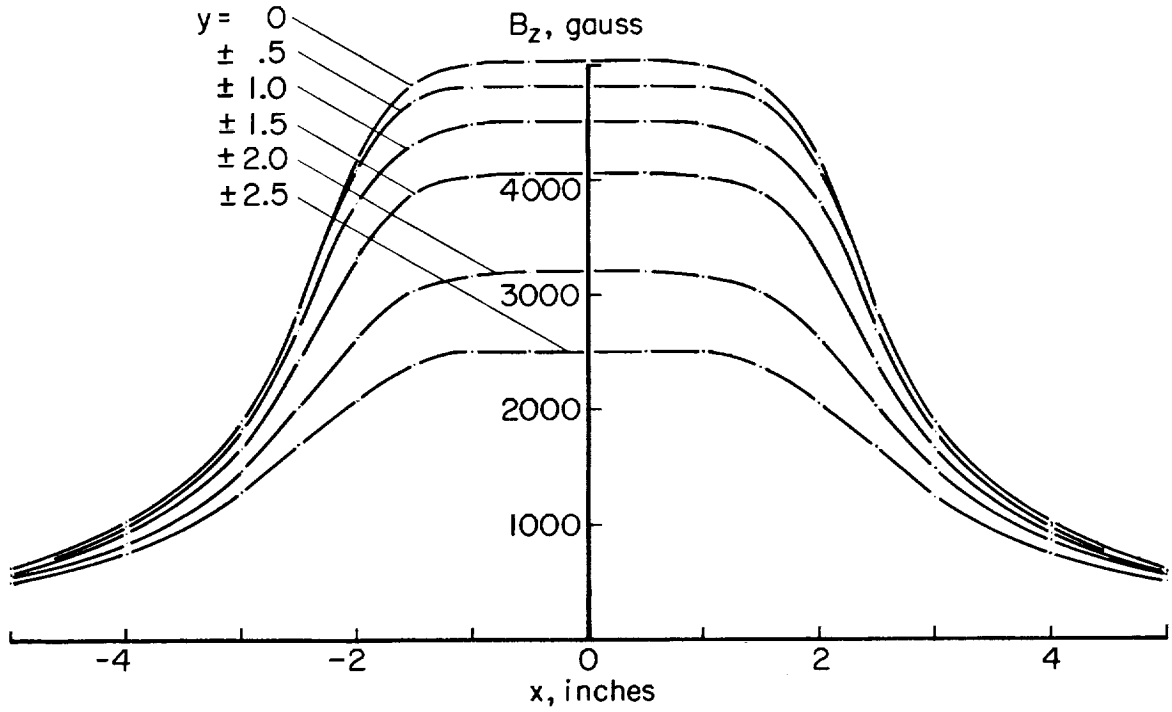

(d) Air gap inserts designed so that $B_z[\psi(l) - \psi(-l)]$ = constant.

Figure 6.- Concluded.

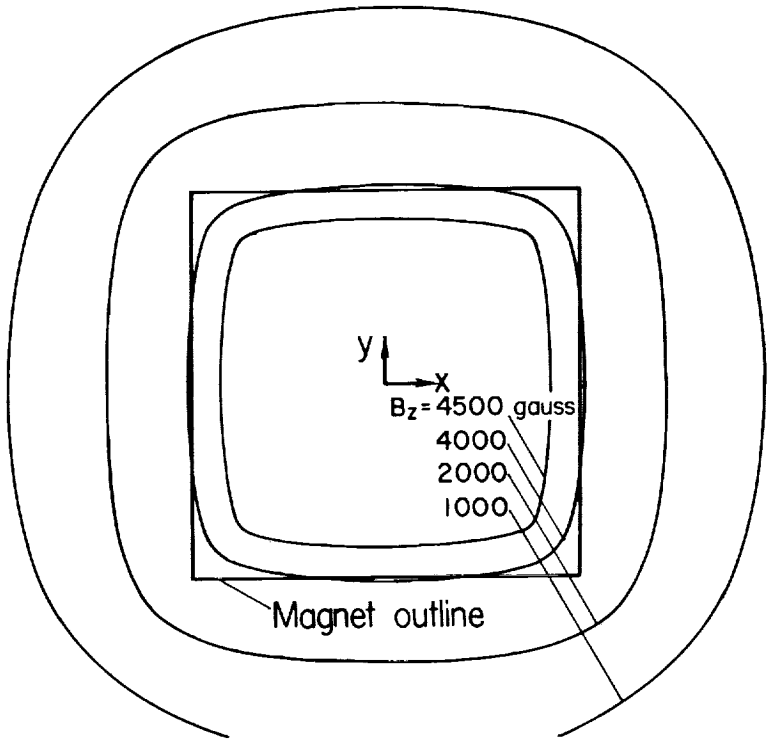

(a) Square pole pieces; 1-1/2-inch air gap.

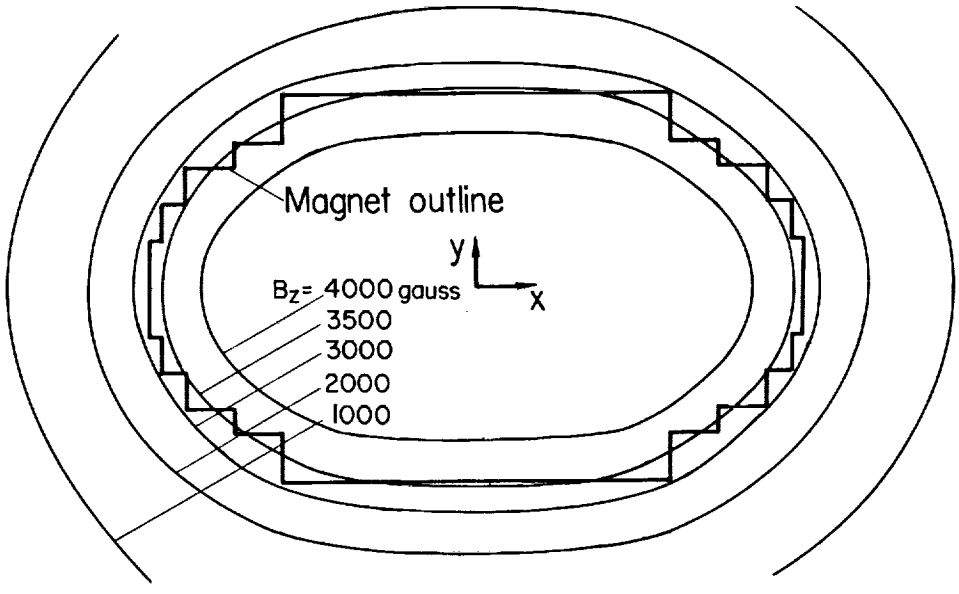

(b) 90 percent contour; 1-1/2-inch air gap.

Figure 7.- Contours of constant magnetic field strength on channel centerplane.

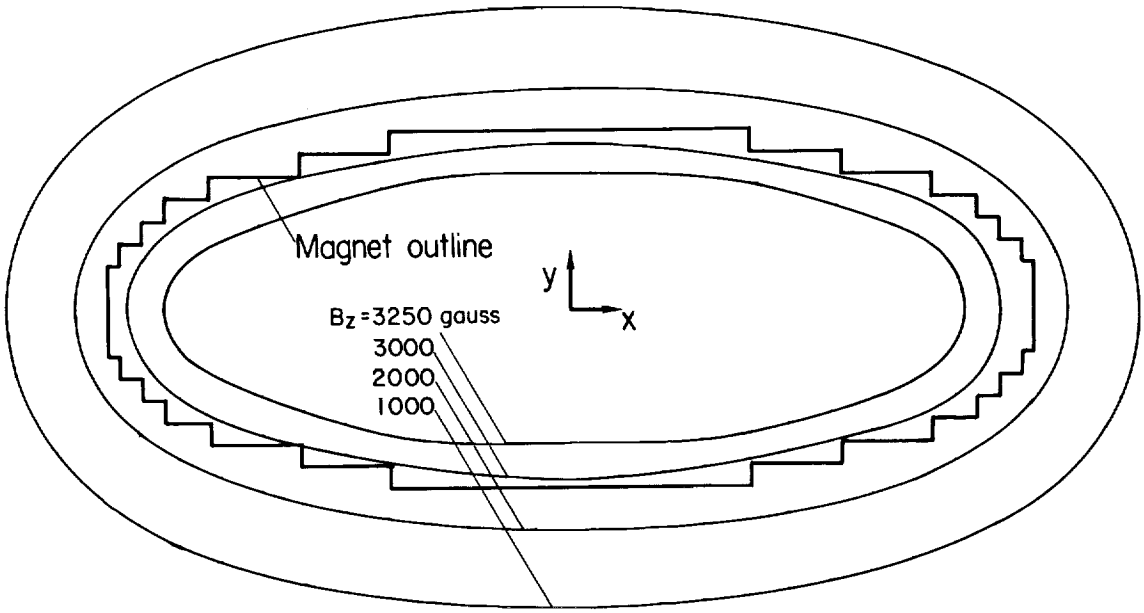

(c) 98 percent contour; 1-1/2-inch air gap.

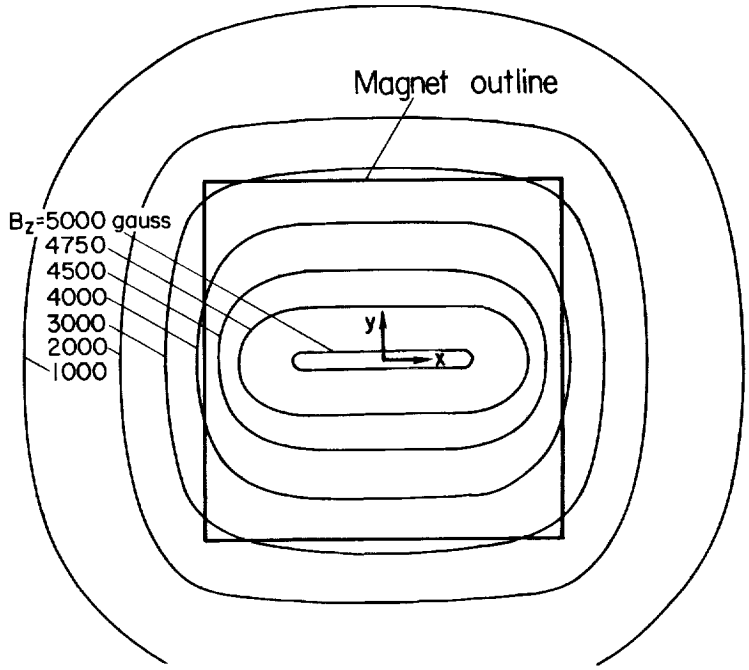

(d) Air gap inserts designed so that $B_z[\psi(l) - \psi(-l)]$ = constant.

Figure 7.- Concluded.

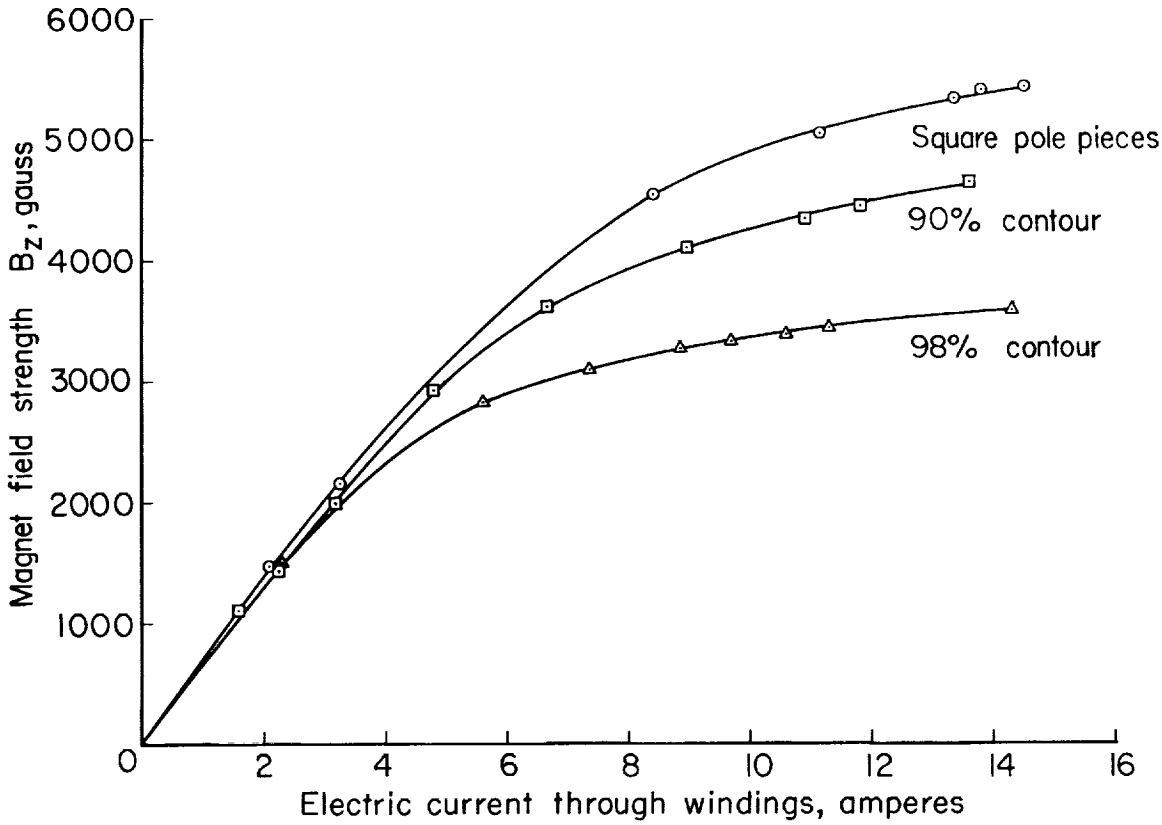

Figure 8.- Field strength of magnet in center of 1-1/2-inch air gap.

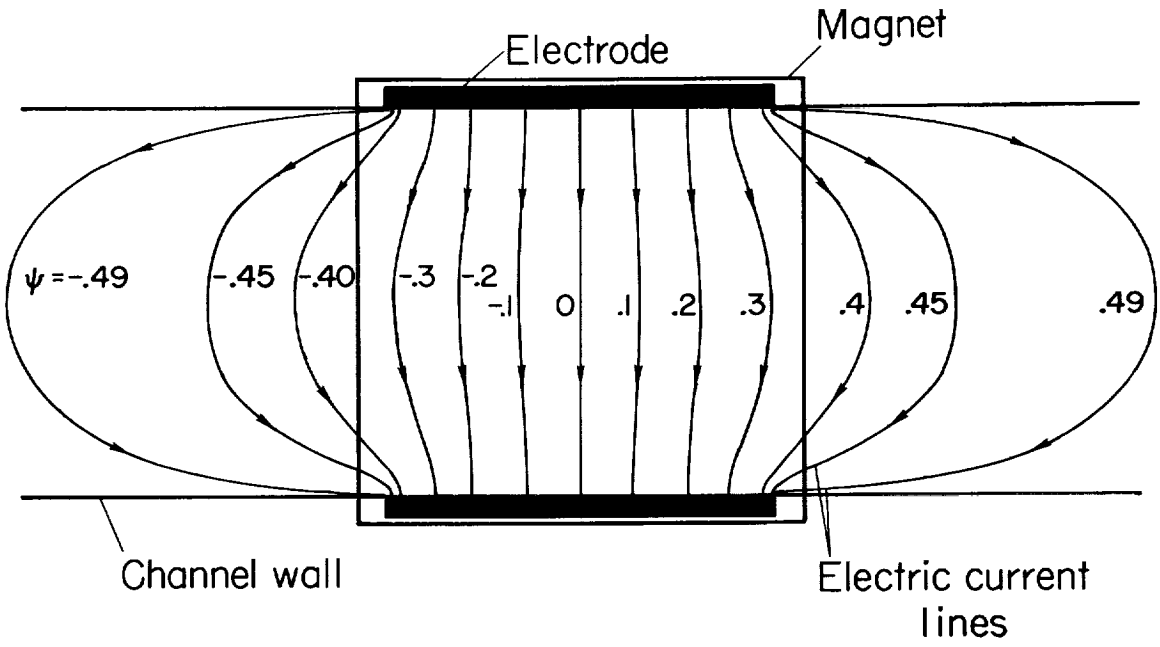

(a) Electric current lines compared with magnet plan form.

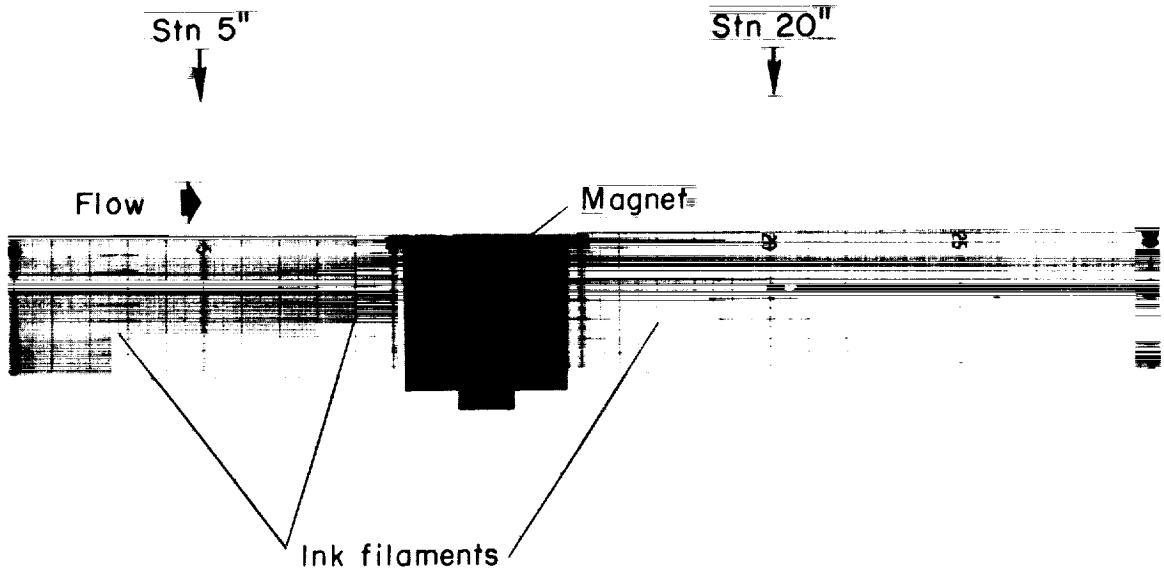

(b) Flow through channel.

Figure 9.- Test channel with 4- by 4-inch magnet and 3-1/2-inch electrodes.

Figure 10.- Flow patterns at zero flow rate.

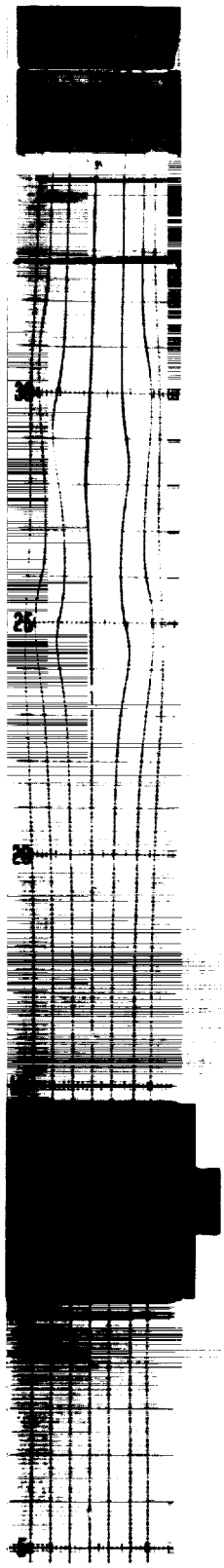

Figure 11.- Flow distortion caused by turning electric or magnetic field on or off.

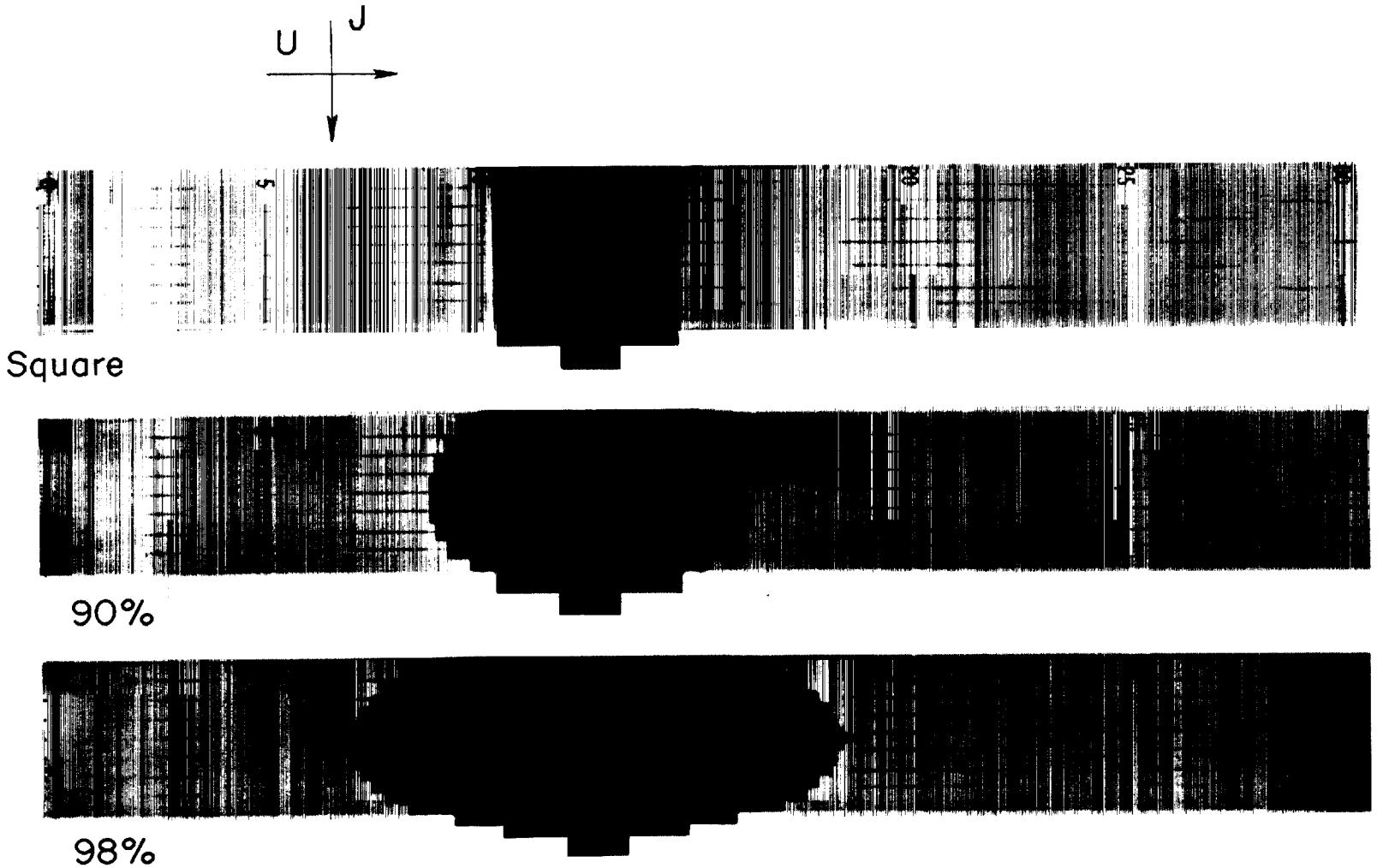

Figure 12.- Ink filament patterns depicting the velocity distribution produced by pumps with special magnet contours and an air gap of 1-1/2 inches.

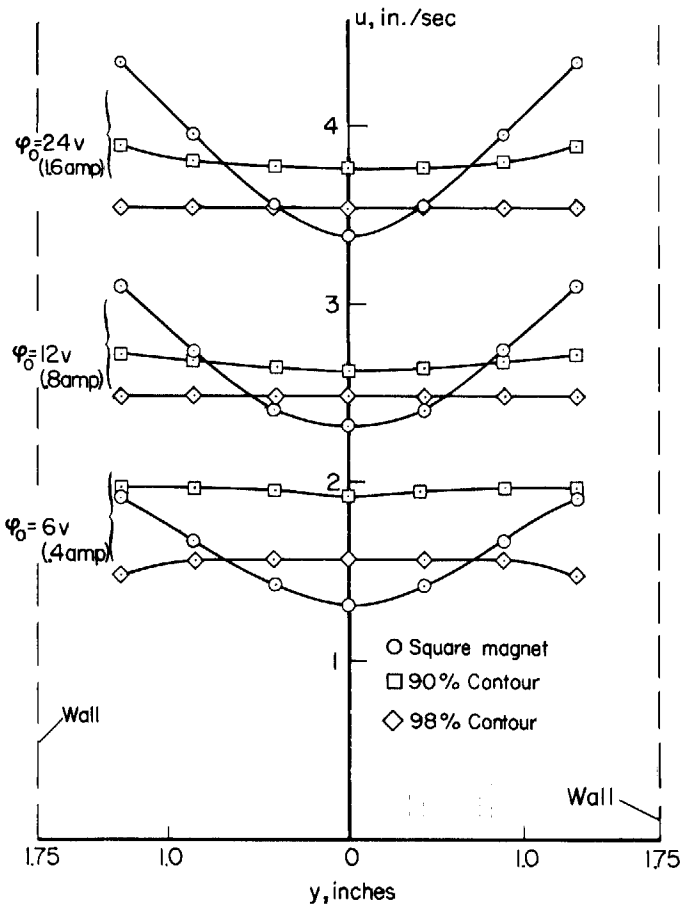

(a) Velocities of ink filaments.

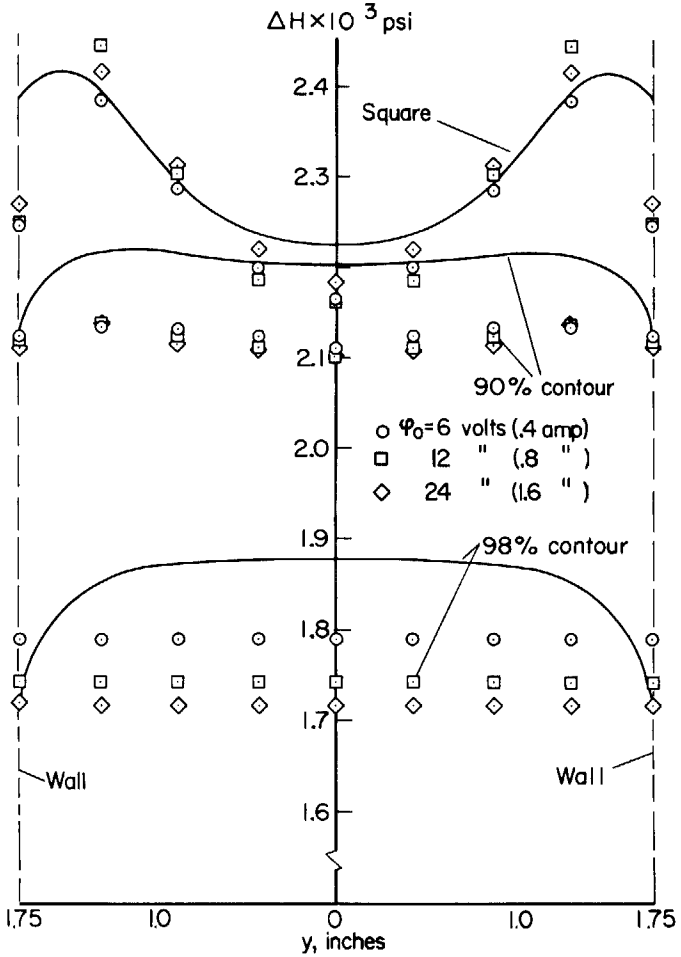

(b) Variation of pressure head in channel; all currents normalized to 1 ampere.

Figure 13.- Measurements at exit of electromagnetic field region; x = 20 inches.

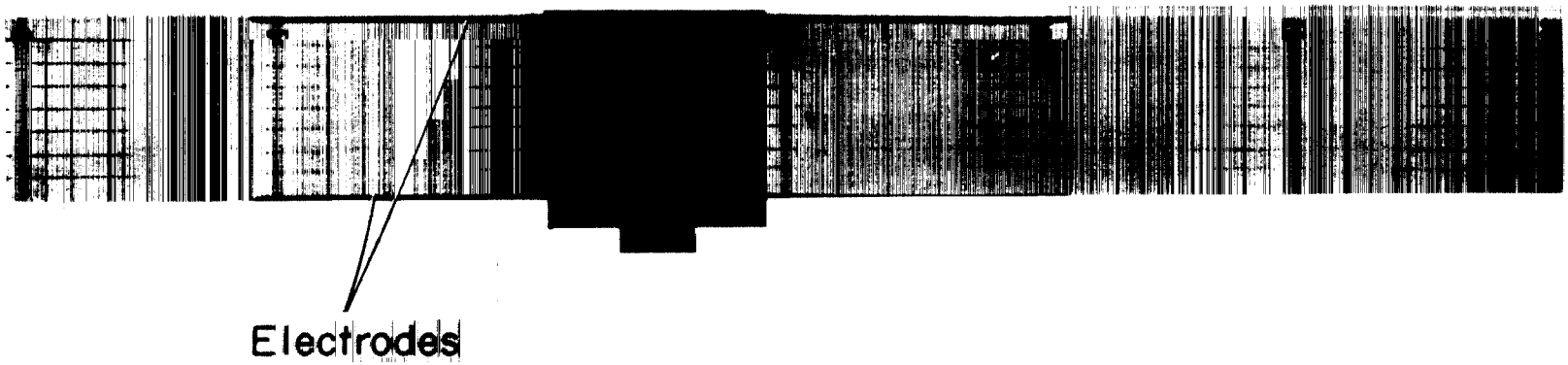

Figure 14.- Uniform flow produced by long electrodes.

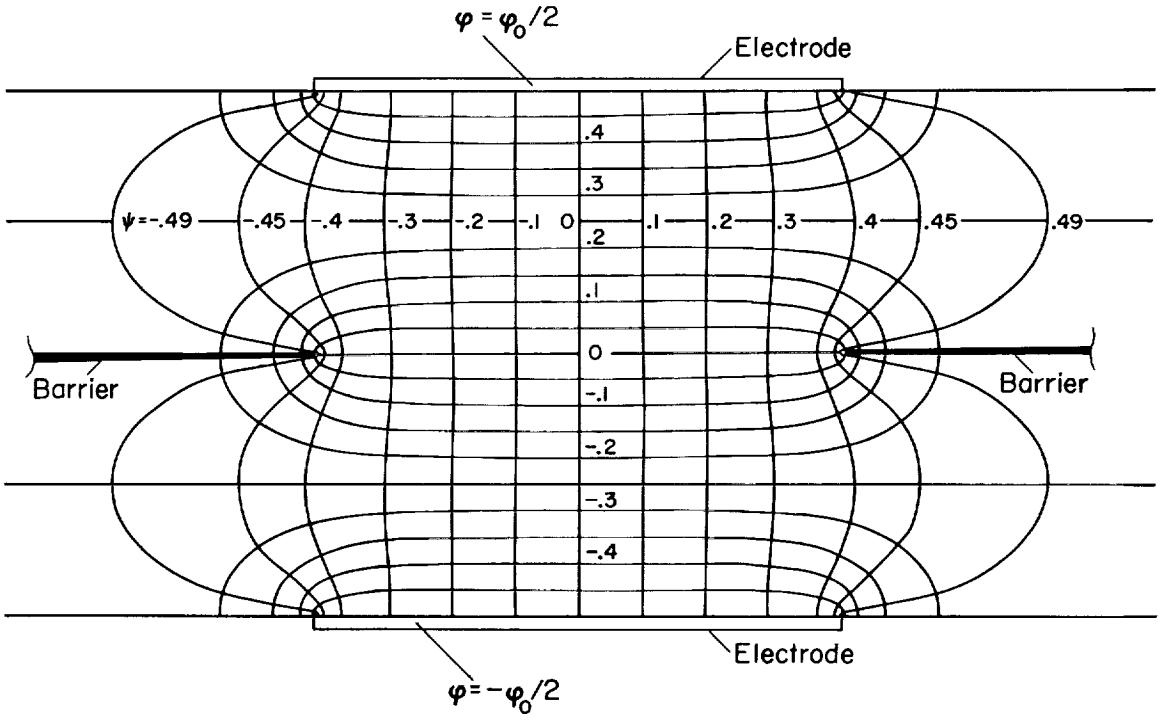

(a) Reduction in fringing of electric field brought about by very long barriers.

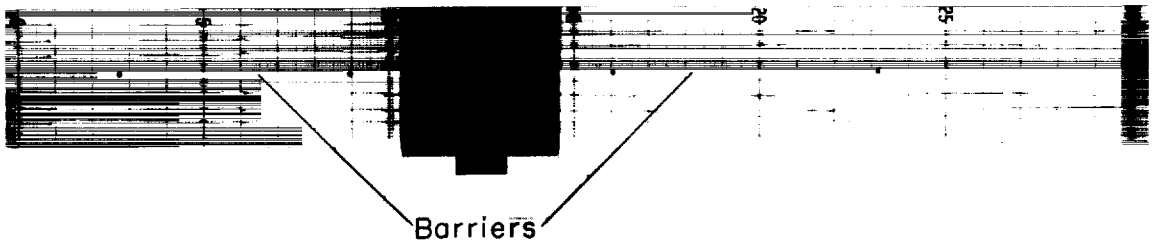

(b) Flow pattern.

Figure 15.- Test channel with 11-inch electric current barriers placed on channel center line.

(a) Constant air gap; $1\frac{1}{2}$"

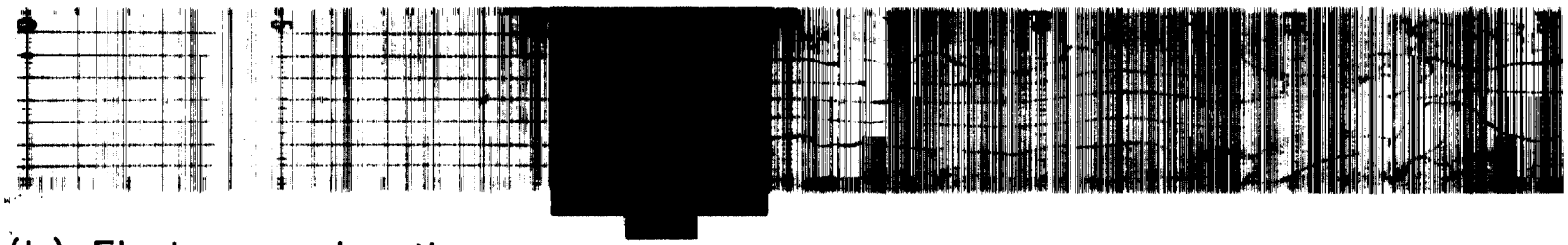

(b) First approximation

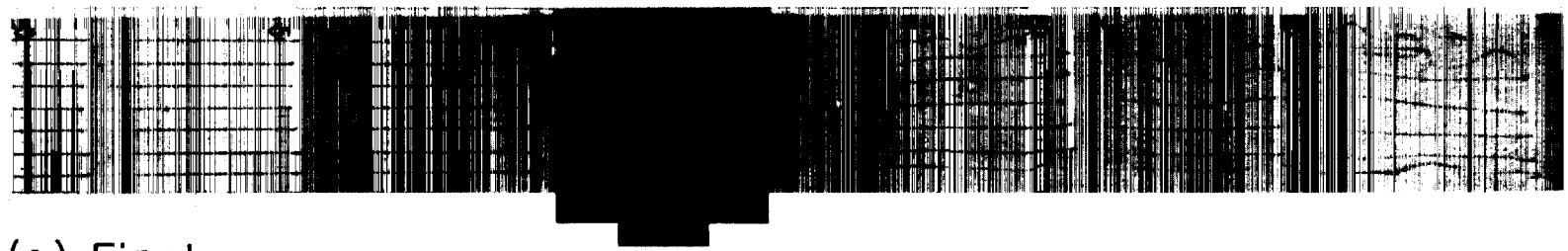

(c) Final

Figure 16.- Flow produced by square magnet with air gap inserts.

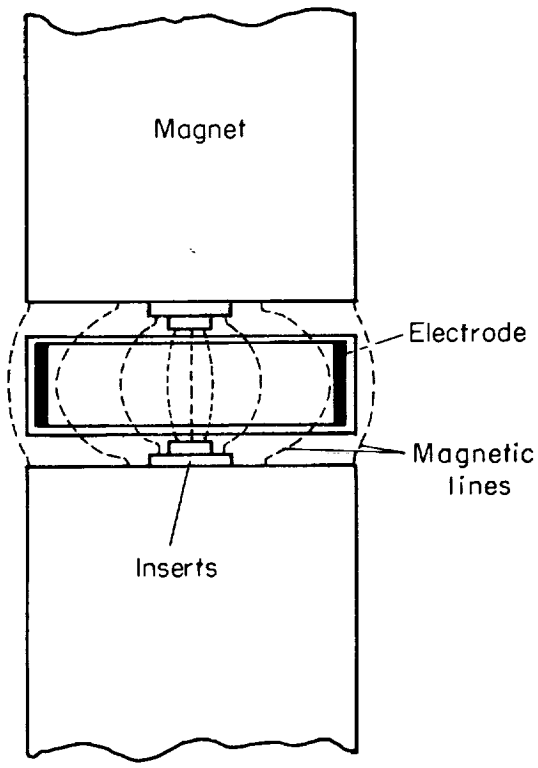

(a) Electrodes unaltered.

Figure 17.- Flow produced by square magnet with 1/8-inch metal slab inserts in the air gap.

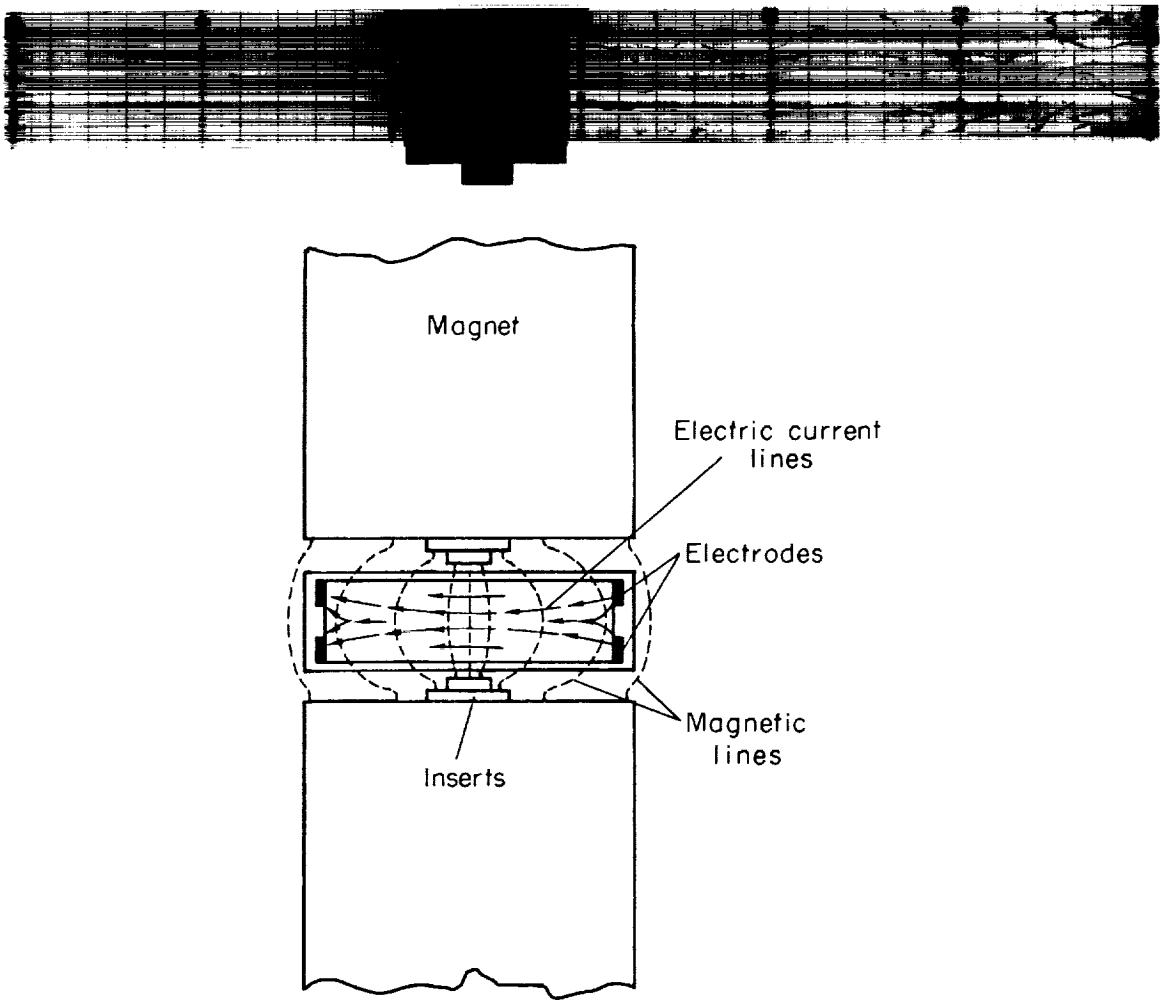

(b) Center part of electrodes removed.

Figure 17.- Concluded.